Brodogradnja Volume 77 Number 3 (2026) 77312

University of Zagreb
Faculty of Mechanical
Engineering and Naval
Architecture

journal homepage: www.brodogradnja.fsb.hr

Brodogradnja

An International Journal of Naval Architecture and
Ocean Engineering for Research and Development

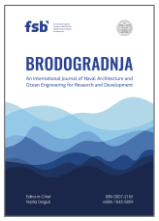

Research on an energy field model for navigation risk assessment of maritime autonomous surface ships incorporating multi-ship interaction features

Zhe Ji, Yingjun Zhang, Jiahui Yang*

Navigation College, Dalian Maritime University, Dalian, 116026, China

ARTICLE INFO

Keywords:
MASS
Multi-ship Interaction
Maritime Traffic Complexity
Navigation Energy Field

ABSTRACT

With the advancement of next generation information technologies, Maritime Autonomous Surface Ships (MASS) are progressively advancing. However, the dynamic uncertainties arising from multi-ship interactions in complex maritime traffic environments significantly constrain their capabilities for risk identification and adaptive switching between Mode(s) of Operation (MoO). To address this challenge, this study proposes a navigation energy field model for risk assessment that integrates multi-ship interaction features. First, maritime traffic complexity is quantified based on intrinsic ship attributes and the Potential Risk Ship Domain (PRSD) framework. Second, to address the inadequacy of conventional field theory in capturing dynamic coupling relationships between ships, a navigation energy field model is developed that incorporating multi-ship interaction characteristics, guided by quantified traffic complexity. Finally, applying the ALARP (As Low As Reasonably Practicable) principle, navigation scenarios are classified, providing a quantitative foundation to support adaptive MoO switching. The results demonstrate that the proposed method effectively reveals the risk evolutionary patterns of collective ship behaviors in multi-ship convergence and high-density traffic environments, thereby enhancing the ability of MASS to identify risks. This research provides theoretical and practical support for risk assessment and adaptive MoO management in MASS, contributing to improved navigational safety under dynamic and complex navigation situations.

1. Introduction

Driven by emerging technologies such as artificial intelligence, big data, and 5G networks, intelligent systems have been widely implemented in fields like maritime and road transportation. Among them, MASS has attracted growing attention within the shipping industry as an innovative solution aimed at reducing human errors [1].

As the International Maritime Organization (IMO) Maritime Safety Committee (MSC) continues to advance the MASS regulatory framework, the definition and operational requirements for MASS related terminology are gradually being standardized and institutionalized. Currently, the IMO has completed several landmark tasks in advancing the development of the MASS regulatory framework: (1) At the 98th MSC, the

* Corresponding author.
E-mail address: zhangyj@dlmu.edu.cn

https://doi.org/10.21278/brod77312
Received 19 October 2025; Received in revised form 14 December 2025; Accepted 12 January 2026
Available online 26 January 2026
ISSN 0007-215X; eISSN 1845-5859

issue of autonomous ships at sea was discussed for the first time, and it was agreed to establish a new deliverable titled “Review of the Regulatory Scope for MASS”; (2) At the 103rd MSC, the task of reviewing the compatibility of existing regulations with MASS was completed;(3) At the 104th MSC, the establishment of a goal based MASS instrument was approved; (4) At the 106th MSC, the MASS Code framework was preliminarily determined, and the roadmap for subsequent development was approved. In addition, with the release of guidance documents such as MSC.1/Circ.1638, important references and policy guidance have been provided for the non-mandatory MASS Code and its related implementation path, which are expected to be introduced in 2028. To standardize the development path of MASS, the 99th MSC classified the autonomous capabilities of MASS into four distinct levels of autonomy [2]. However, in actual operation, the levels of autonomy of MASS are not constant but are affected by external environmental factors, requiring MASS to switch in real-time during operation, which limits the application of the original static classification method in complex environments.

To address this challenge, the 107th MSC further proposed replacing the conventional autonomy level classification with the concept of Mode(s) of Operation (MoO), to dynamically define the ship’s level of autonomy [3]. This definition reflects the current technical limitations of MASS, namely their inability to fully handle complex and rapidly changing maritime conditions. Consequently, MASS still rely on remote control and onboard crew as redundant safeguards to enhance their responsiveness and handling capability in diverse navigation scenarios.

Against this backdrop, enhancing the dynamic risk perception capability of MASS with respect to navigational environment complexity has become a key prerequisite for achieving adaptive switching between MoO [4]. At present, the core focus of MASS development lies in advancing autonomous perception [5] and decision-making [6, 7], aiming to strengthen their autonomous operation in complex navigational environments. Network based methods such as Bayesian have been widely applied in modeling uncertain ship behavior and have played an important role in the MASS risk assessment framework [8]. Meanwhile, the International Regulations for Preventing Collisions at Sea (COLREGs) have been integrated into the path planning and collision avoidance decision-making processes of MASS, to ensure regulatory compliance and the safe operation of their navigation systems [9, 10]. However, these methods typically focus on rule consistency or probabilistic reasoning and remain inadequate in modeling the spatiotemporal evolution of potential risks in complex multi-ship interaction scenarios. There remains a significant gap in research concerning risk assessment of navigational scenarios. Specifically, since there is a lack of a quantitative evaluation model centered on MASS that can dynamically reflect the complexity of its current operating environment. This gap is particularly evident in a typical high complexity scenarios such as multi-ship encounters and high-density traffic flows, where traditional risk warning systems struggle to effectively capture the interactions between vessels and the spatiotemporal evolution of potential risk areas. These limitations not only hinder MASS’s understanding of environmental changes but also weaken its ability to achieve adaptive switching between different MoO.

To address this issue, field-based methods have been widely applied in the domain of maritime navigation risk assessment in recent years [11]. These methods regard vessels as dynamic field sources, using navigation energy fields to describe their influence on the surrounding environment, thereby reflecting the distribution of potential risks and behavioral trends. Although existing navigation energy field models have improved, the visualization and quantification of navigational risk, most models still treat elements within the scenario as independent of each other, hence fail to adequately consider the interactions and potential coupling relationships between multiple vessels when constructing the navigation energy field. While such simplified modeling strategies are somewhat applicable in low density traffic environments, they struggle to accurately capture the dynamic characteristics and risk evolution trends in complex scenarios such as multi-ship encounters and high-density traffic. This limitation is particularly pronounced in applications targeting MASS, where the generalization and adaptability of these models require urgent enhancement.

To sum up, although existing research has made positive progress in ship collision risk assessment and maritime traffic situation modeling, the following key gaps remain: (1) Most maritime traffic risk research is conducted from a regulatory perspective and lacks dynamic risk quantification methods that focus on

individual ships and reflect the characteristics of multi-ship interactions.(2) Although existing navigation energy field models have improved the visualization and quantification of navigation risks to a certain extent, they cannot effectively characterize the coupled effects of multi-ship interaction behavior on risk evolution. (3) Existing MASS navigation risk assessment methods overlook the basis for determining the risk levels required for switching between different MoO in complex dynamic scenarios. Therefore, there is an urgent need to develop a navigation scenario risk quantification model that integrates traffic flow evolution characteristics, interactions between ships, and potential conflict risks to provide reliable support for MASS autonomous cognition, risk assessment, and MoO adaptive switching, thereby enhancing its autonomous navigation capabilities and safety assurance in complex dynamic environments.

To develop a risk assessment model suitable for MASS navigation characteristics, it is crucial to obtain comprehensive and reliable maritime traffic data. It is worth noting that, according to IMO regulations, since 2015, all ships of 300 gross tonnage or more navigating in international waters and all passenger ships of any tonnage must be equipped with an Automatic Identification System (AIS). The widely deployed AIS has not only significantly improved maritime traffic safety but also provided critical data support for ship behavior modeling, multi-ship interaction feature analysis, and navigation risk assessment [12]. Therefore, this paper selects a portion of AIS data for ship navigation risk assessment in the model validation section to verify the applicability and effectiveness of the proposed navigation energy field model in actual complex maritime environments.

In summary, this study aims to develop a navigation energy field model for risk assessment that incorporates multi-ship interaction characteristics. This research not only contributes to a deeper understanding of the risk evolution patterns in collective vessel behavior within complex traffic environments but also provides theoretical support and algorithmic foundations to support adaptive MoO switching, thereby advancing its practical applications in autonomous perception and risk assessment. The main contributions of this study are summarized as follows:

1) A maritime traffic complexity measurement method tailored to multi-ship interaction scenarios is proposed based on the intrinsic attributes of vessels and the Potential Risk Ship Domain (PRSD) theory [13]. Inspired by ji et al. [14], this method quantifies potential collision risks from three dimensions—density complexity, proximity complexity, and mitigation complexity—with the objective of enhancing MASS's risk perception capability in complex navigational environments and laying the foundation for constructing the navigation energy field potential function.

2) A coupled navigation energy field model has been developed that integrates maritime traffic complexity metrics into potential function calculations. Unlike traditional field-based approaches treating proximity and interaction density as independent factors, the proposed model embeds complexity values as parameters within Gaussian potential terms. This dynamically captures the interaction characteristics and risk evolution trends between vessels within the traffic environment, thereby significantly enhancing the expressive capability and applicability of risk assessment in complex navigation scenarios.

3) A classification standard for navigational scenario risk levels is defined by leveraging the As Low As Reasonably Practicable (ALARP) principle [15], along with a quantitative foundation to support adaptive MoO switching. This contribution enhances its adaptability and safety assurance capabilities in complex and dynamic navigational environments.

The rest of this paper is organized as follows: Section 1 reviews related work; Section 2 introduces the maritime traffic complexity measurement model, constructs the navigation energy field, and defines the classification principle for navigational scenario risk levels; Section 3 presents a case study to validate the effectiveness of the proposed model; Section 4 discusses the limitations of the model and outlines directions for future improvements; and finally Section 5 concludes the study with final remarks and conclusions.

2. Literature review

In actual maritime operations, one of the key challenges faced by ship operators or autonomous systems is the accurate assessment of potential collision risks among vessels [16]. Since MASS typically operate under

two distinct MoOs—"autonomous" and "remote operation"—their understanding of the external navigational environment and risk perception capabilities are directly linked to decision-making safety and the system's ability to achieve adaptive MoO switching [17].

When operating in autonomous mode, collision risk identification relies entirely on the onboard perception system's real-time processing of information regarding surrounding dynamic entities (e.g., nearby vessels), including their positions, velocities, and movement trends. The system must comprehensively analyze the current traffic situation, identify potential risk areas, and formulate appropriate collision avoidance strategies. If the actual risk exceeds the system's predefined handling capacity or if the scenario complexity surpasses its cognitive threshold, a control switching mechanism must be promptly activated to transfer control from the autonomous system to shore based operators or onboard crew, thereby ensuring navigational safety.

In the field of maritime navigation risk assessment, various quantitative methods have been proposed, incorporating parameters such as the Distance to Closest Point of Approach (DCPA), Time to Closest Point of Approach (TCPA), and Collision Risk Index (CRI). Ship operators or autonomous systems can dynamically monitor navigational situations and identify risks by establishing corresponding risk thresholds based on these parameters, thereby facilitating collision avoidance warnings [18]. However, these methods generally rely on the assumption of "constant speed and heading," implying that both the target ship and the own ship are presumed to maintain constant speed and course. While this assumption simplifies the collision risk calculation model, it overlooks the frequent changes in speed and course encountered in real-world navigation scenarios, which consequently affects the accuracy and timeliness of risk assessments [19].

The Ship Domain (SD), introduced by Fujii and Tanaka [20], offers a novel perspective for assessing collision risk between vessels. SD represents a generalized safe distance around a ship, defining a spatial zone within which other vessels should not intrude, thereby establishing the navigational safety boundary. Compared to conventional parameters such as DCPA, TCPA, and CRI, SD enables real-time and spatial visualization of potential collision risks. However, while SD provides valuable insight into relative vessel safety, it does not indicate the precise timing of a potential collision. Consequently, in complex maritime traffic environments, SD serves primarily as a reference tool and cannot be solely relied upon as a definitive basis for decision-making.

In order to more effectively reflect the interactions between multiple ships in the maritime traffic environment, scholars have gradually introduced the perspective of complexity science, viewing maritime traffic systems as dynamically evolving complex networks, thereby expanding the theoretical understanding and modeling capabilities of risk generation mechanisms. Wen et al. [21] proposed and developed a complexity measurement model based on intrinsic vessel attributes, quantitatively evaluating maritime traffic complexity by integrating factors such as vessel density, speed, and relative distance. However, this model primarily focuses on pairwise vessel interactions and is less effective in capturing multi-vessel traffic dynamics across entire waterways. Sui et al. [22] applied a complex network approach to quantify maritime traffic dynamics, characterizing the system's evolution through topological features such as degree, clustering coefficient, and structural entropy. Liu et al. [23] established a dynamic complexity model based on radial distribution functions of vessel speed, heading, and position, integrating these to derive an overall complexity indicator. This method emphasizes the relationship between spatial distribution patterns and microlevel state changes, demonstrating strong identification capabilities; however, its representation of multivessel dynamic interactions remains relatively simplified. Sui et al. [24] proposed a traffic complexity measurement method combining Voronoi diagrams with complex networks, effectively eliminating the need to predefine safety distances. Zhang et al. [25] introduced the Rule based Maritime Traffic System Complex Network (RMTSCN) model, which incorporates COLREGs rules and utilizes metrics such as node degree and vertex strength to capture the evolution of traffic system complexity, thus enhancing the digitalization of Vessel Traffic Services (VTS). Tong et al. [26] employed an improved WVoteRank algorithm to identify key vessels in multi-vessel encounter scenarios and conducted clustering based on spatial compactness and risk connectivity, improving the recognition of complex traffic zones. Ji et al. [14] developed a multi-vessel traffic complexity assessment model incorporating vessel density, proximity factor, and mitigation index, offering a more comprehensive reflection of potential risks in maritime traffic situations. Experimental results demonstrated its strong

capability in identifying potential collision risks. In recent years, with the gradual deepening of the application of complexity science in the field of shipping, particularly in the assessment of maritime traffic situations. By incorporating methodologies such as complex networks, social force models, and multilayer networks, researchers have enabled multi-scale and multi-dimensional dynamic analyses of vessel traffic conditions, offering valuable insights into the underlying patterns and potential risks within traffic systems. However, existing studies predominantly focus on overall waterway characteristics or general multi-vessel interaction patterns, while research concerning localized risk perception, dynamic situational changes, and decision-making relevance for individual vessels operating in complex environments remains relatively limited. This gap hinders the ability to meet the increasing demand for fine grained risk identification, which is essential for the development of MASS.

To address this research gap, field theory has recently been introduced as a novel modeling approach in the maritime traffic domain [27]. By leveraging the continuous spatial distribution characteristics of field theory, dynamic navigation environments can be abstracted as energy fields [28, 29], which describe the risk distribution around the own ship by comprehensively considering the motion states of target ships, traffic density, and the intrinsic properties of the own ship. Like Lazarowska, based on static and dynamic obstacles, a discrete potential field model was constructed for ship path optimization, and the feasibility of trajectories compliant with COLREGs was improved through path optimization algorithms [30]. Lyu et al. constructed an accurate potential field model coupling static and dynamic obstacles, significantly improving the feasibility of multi-ship collision avoidance in complex navigation environments [31]. Additionally, DiArchangel optimized potential field parameters using a genetic algorithm, enhancing the robustness of path planning in multiship intersection scenarios [32]. Compared to traditional methods, navigation energy field models offer enhanced spatiotemporal dynamic representation capabilities and better align with the local perception mechanisms relied upon by ship operators or autonomous systems during real-world operations. However, existing navigation energy field models still exhibit certain limitations. On one hand, their potential field functions of the navigation energy field typically adopt unified global parameters, lacking detailed quantification of individual vessel perception differences in complex scenarios. On the other hand, these models often focus on local interactions between the own ship and a single target ship, overlooking the holistic impact of multi-ship interaction behaviors within the overall traffic network on the navigation energy field distribution.

In terms of MoO research progress in MASS, since the IMO first proposed the MoO concept at the 107th MSC, related research has gradually focused on the state recognition and dynamic response capabilities of MASS in complex and variable maritime environments. The introduction of MoO aims to provide an adaptable operational framework for Autonomous Navigation Systems (ANS) so that the system can flexibly switch between different levels of autonomy based on environmental perception results. Zhang et al. proposed a MoO switching framework based on the Degree Two of MASS (MASS-DoA2) system, combining expert surveys to construct control mode option paths for MASS in different scenarios [33]. Rodseth et al. proposed a risk-driven MoO approval mechanism from the perspective of operational envelope [17]. Furthermore, Li et al. analyzed the risk evolution characteristics of MASS under different MoO states based on the System Theoretic Process Analysis- Hidden Markov Model (STPA-HMM) composite framework, clearly identifying “traffic complexity” and “traffic density” as the key factors triggering mode switching [34]. Tomohiro constructed a MASS risk analysis classification framework to provide theoretical support to the MoO switching mechanism [35]. However, existing research is mainly based on expert knowledge and rule-based judgment and lacks unified quantitative evaluation criteria. In particular, in scenarios with multiple ships and high-density interactions, a stable and effective dynamic switching evaluation system has not yet been developed. Therefore, it is necessary to develop MoO switching methods based on risk quantification and maritime traffic complexity modeling to enhance the mode adaptation ability and operational safety of MASS in dynamic environments.

To further address the limitations of existing ship navigation risk assessment methods in complex traffic environments, this study proposes a navigation energy field model integrated with maritime traffic complexity. Grounded in the intrinsic attributes of vessels and the PRSD theory, the model incorporates density, proximity

factor, and mitigation index to develop a complexity measurement method suitable for multi-ship interaction scenarios. This enables the quantitative characterization of local situational complexity faced by individual vessels. Unlike conventional navigation field theory models that treat each vessel as an independent field source, this study innovatively integrates the coupling relationships among vessels—derived from maritime traffic complexity—into the navigation energy field construction process. By doing so, it establishes a dynamic risk quantification model based on individual vessel heterogeneity and interaction characteristics. This approach facilitates dynamic identification and quantification of risk evolution in high-density, multi-ship interaction environments. Furthermore, based on the ALARP principle, the study defines a risk-level classification standard for navigation scenarios and provides recommended MoO for MASS under different risk levels. This offers quantitative guidance and theoretical support for adaptive switching of MoO in complex dynamic environments. The specific research framework is illustrated in Figure 1.

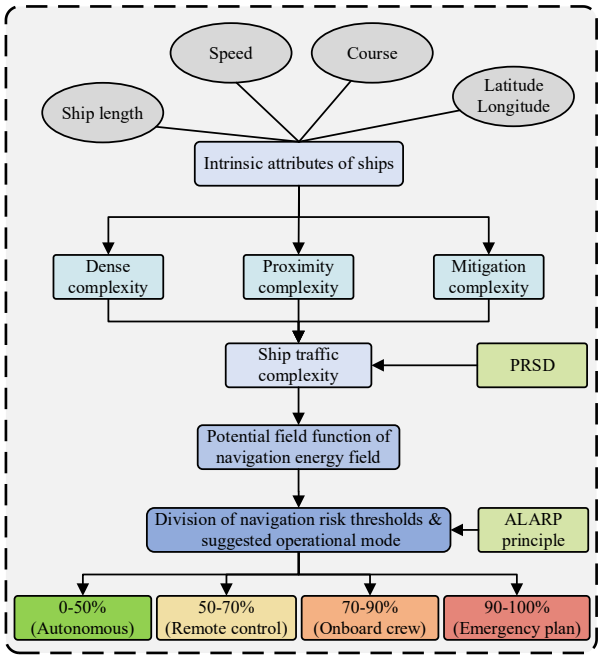

Fig. 1 Research roadmap

3. Methodology

The proposed methodology in this study comprises three main components: First, the calculation of maritime traffic complexity under multi-ship interactions to characterize the local risk features faced by vessels in complex navigation environments; Second, the construction of a potential function for the navigation energy field based on the developed complexity metrics and principles of field theory, enabling dynamic modeling of the navigation energy field; and finally, the classification of navigation scenario risk levels in accordance to the ALARP principle, providing a foundation for the dynamic switching of MoO. This structured approach ensures comprehensive risk assessment and adaptive operational adjustments in dynamic maritime environments.

3.1 Calculation of maritime traffic complexity

3.1.1 Maritime traffic complexity calculation for pairwise ships

Inspired by Ji et al. [14], the complexity between pairwise ships in a maritime traffic scenario can be analyzed from three perspectives: density complexity $den_{ij}(t)$, proximity complexity $pv_{ij}(t)$ and mitigation complexity $ev_{ij}(t)$.

The metric $den_{ij}(t)$ quantifies the complexity arising from ship density, with higher traffic density leading to larger values, as detailed in Equations (1) and (2):

$$den_{ij}(t) = e^{-\alpha\frac{\left|\overrightarrow{d_{ij}(t)}\right|}{R_{ij}}} \tag{1}$$

$$\left|\overrightarrow{d_{ij}(t)}\right| = 2r\arcsin\left(\sqrt{\sin^2\left(\frac{lat_j - lat_i}{2}\right) + \cos(lat_i)\cos(lat_j)\sin^2\left(\frac{lon_j - lon_i}{2}\right)}\right) \tag{2}$$

In the equations, α is a calibration parameter dependent on the navigational environment; $\left|\overrightarrow{d_{ij}(t)}\right|$ denotes the relative distance between ships i and j at time t; R_{ij} determined by ship type and environmental conditions. lon_i and lat_i represent the longitude and latitude of ship i, while lon_j and lat_j correspond to those of ship j. r is the radius of the Earth, taken as 3,440 nautical miles (nm).

The calculation of $den_{ij}(t)$ involves two key parameters, α and R_{ij}. To determine the validity of the value assigned to these parameters, a sensitivity analysis was conducted, with the results presented in Figure 2.

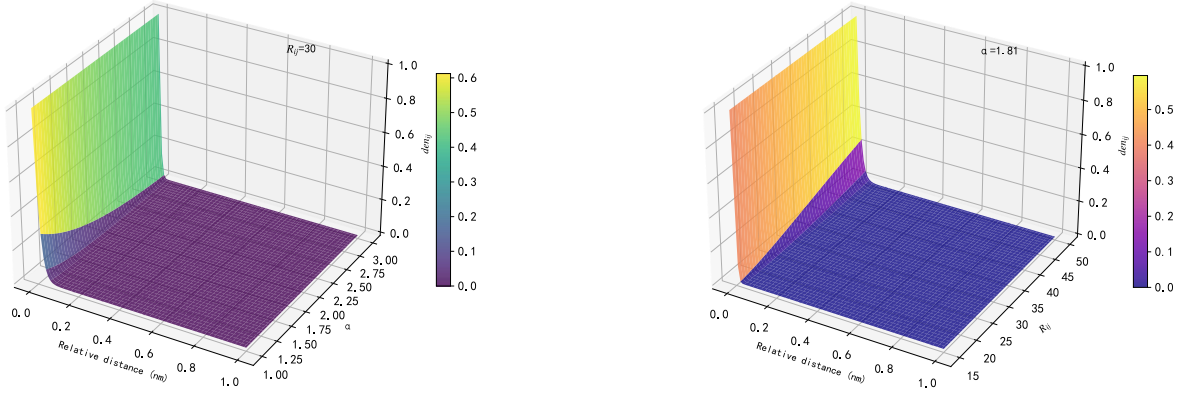

(a) (b)

Fig. 2 Sensitivity analysis of key parameters for $den_{ij}(t)$

Figure 2(a) illustrates the effect of varying alfa values on $den_{ij}(t)$ when R_{ij} is fixed at 30, whilst Figure 2(b) demonstrates the impact of different R_{ij} values when α is fixed at 1.81. The results indicate that as R_{ij} decreases, $den_{ij}(t)$ exhibits exponential growth. Different combinations of α and R_{ij} can be used to fit distinct growth curves, providing a theoretical basis for parameter adjustment when considering the differential impact of varying vessel types and navigational environments on interaction intensity in future studies. To enhance the model's universality and comparability, vessels are uniformly treated as a "standard ship" – specifically a bulk carrier with a deadweight of 70,000 tonnes, length of 230 metres, and width of 32.3 metres. This defines the fundamental scale for parameters related to traffic complexity modelling [36]. Building upon the research of Wen et al. [21], extensive numerical experiments validated the final parameter settings: R_{ij} set to 30, and α at 1.81. This parameter combination not only ensures consistency with the value ranges of other complexity metrics but also effectively reflects the intensity of ship-to-ship interactions.

The $pv_{ij}(t)$ quantifies the influence of the relative motion trend between two ships on maritime traffic complexity at time t. It incorporates four key parameters: the spatial convergence factor $cv_{ij}(t)$, the temporal convergence factor $tv_{ij}(t)$, the ship safety distance $d_{safedis}$, and the relative distance between ships $\left|\overrightarrow{d_{ij}(t)}\right|$.

When $cv_{ij}(t) < 0$, it indicates that the two ships are in a converging state, as defined in Equation (3):

$$cv_{ij}(t) = v_j(t)(\alpha_x(t)\sin(\theta_j(t)) + \alpha_y(t)\cos(\theta_j(t))) - v_i(t)(\alpha_x(t)\sin(\theta_i(t)) + \alpha_y(t)\cos(\theta_i(t))) \tag{3}$$

In the equation, $v_i(t)$ and $v_j(t)$ represent the speeds of ships i and j at time t, respectively; $\theta_i(t)$ and $\theta_j(t)$ denote the headings of ships i and j at time t; $\alpha_x(t) = \frac{lon_j(t)-lon_i(t)}{|\overrightarrow{d_{ij}(t)}|}$ and $\alpha_y(t) = \frac{lat_j(t)-lat_i(t)}{|\overrightarrow{d_{ij}(t)}|}$.

The $tv_{ij}(t)$ describes the degree of approach between ships and the urgency of their convergence. When the convergence situation becomes more severe, its value decreases accordingly, as defined in Equation (4):

$$tv_{ij}(t) = \frac{|\overrightarrow{d_{ij}(t)}|}{cv_{ij}(t)} \tag{4}$$

The $d_{safedis}$ is calculated based on the improved PRSD proposed by Zou et al. [37]. The SD is modeled as an eccentric ellipse, and its safety boundary is computed using Equation (5):

$$\begin{cases} D_{\varphi} = \sqrt{-2\times\ln(PCR)}\times v_i(t)\times\delta\times L_i & if \quad D_{\varphi fr} \le D_{\varphi af} \\ D_{\varphi fr} = \sqrt{\dfrac{-2\times\ln(PCR)}{\lambda v_i(t)^2 \sin{\varphi_p}^2 + \cos{\varphi_p}^2}}\times v_i(t)\times\delta\times L_i & if \quad 0^\circ \le \varphi_p < 90^\circ \text{ or } 270^\circ < \varphi_p \le 360^\circ \\ D_{\varphi af} = \sqrt{\dfrac{-2\times\ln(PCR)}{\lambda v_i(t)^2}}\times v_i(t)\times\delta\times L_i & if \quad 90^\circ \le \varphi_p \le 270^\circ \end{cases} \tag{5}$$

In the equation, D_{φ}, $D_{\varphi fr}$ and $D_{\varphi af}$ represent the whole, fore and aft boundaries of the SD, respectively; φ_p denotes the angle between point p and the ship's heading; L_i is the length of the ship; λ and δ are the lateral and longitudinal influence parameters of the SD, respectively; and PCR indicates the potential collision risk index.

The SD calculated by Equation (5) is illustrated in Fig. 3. In this example, the ship has a speed of 11 knots and a length of 200 meters. The green area in Fig. 3 represents the SD range adopted in this study.

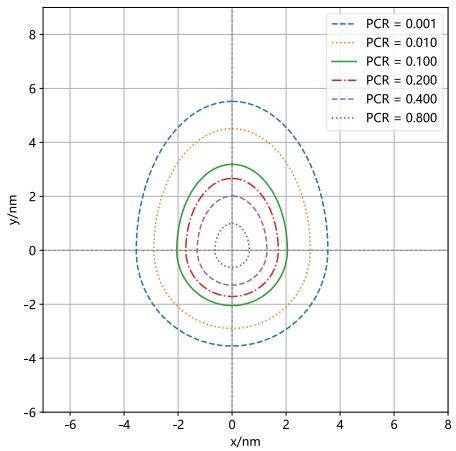

Fig. 3 Schematic diagram of the SD

To sum up, the $pv_{ij}(t)$ between ships can be expressed by Equation (6):

$$pv_{ij}(t) = \begin{cases} \dfrac{1}{1+e^{ktv_{ij}(t)}}\left(1+\dfrac{d_{safedis}}{|\overrightarrow{d_{ij}(t)}|}\right) & cv_{ij}(t) < 0 \\ \dfrac{1}{1+e^{ktv_{ij}(t)}}\left(1+\dfrac{d_{safedis}}{|\overrightarrow{d_{ij}(t)}|^{\tau}}\right) & cv_{ij}(t) \ge 0 \end{cases} \tag{6}$$

In the equation, k and τ are adjustment parameters, which are set to $k = 10$ and $\tau = 2$, the basis for selecting parameter values and specific explanations can be found in the relevant methods and experimental results presented by Ji et al [14].

The $ev_{ij}(t)$ measures the operational difficulty of a single ship in response to the current traffic situation in its surrounding waters. This indicator comprehensively considers the relative motion relationship between ships, the own intrinsic properties of the own ship, and its interactions under specific traffic conditions, providing a quantitative description of the traffic decongestion difficulty for a single ship at time *t*. The detailed formulation is presented in Equation (7):

$$ev_{ij}(t) = \left|\overrightarrow{\nabla cv_{ij}(t)}\right| = \left\| \left[\frac{\partial cv_{ij}(t)}{\partial v_i}, \frac{\partial cv_{ij}(t)}{\partial v_j}, \frac{\partial cv_{ij}(t)}{\partial \theta_i}, \frac{\partial cv_{ij}(t)}{\partial \theta_j} \right]^T \right\| \tag{7}$$

To sum up, the complexity between pairwise ships can be quantitatively described by $den_{ij}(t)$, $pv_{ij}(t)$ and $ev_{ij}(t)$, as shown in Equations (8) and (9):

$$a_{ij}(t) = den_{ij}(t) + pv_{ij}(t) + ev_{ij}(t)^{-1} \tag{8}$$

$$a_{ij}(t) = \begin{cases} e^{-\alpha \frac{\left|\overrightarrow{d_{ij}(t)}\right|}{R_{ij}}} + \frac{1}{1+e^{ktv_{ij}(t)}}\left(1 + \frac{d_{safedis}}{\left|\overrightarrow{d_{ij}(t)}\right|}\right) + \left\| \left[\frac{\partial cv_{ij}(t)}{\partial v_i}, \frac{\partial cv_{ij}(t)}{\partial v_j}, \frac{\partial cv_{ij}(t)}{\partial \theta_i}, \frac{\partial cv_{ij}(t)}{\partial \theta_j} \right]^T \right\|^{-1} & cv_{ij}(t) < 0 \\ e^{-\alpha \frac{\left|\overrightarrow{d_{ij}(t)}\right|}{R_{ij}}} + \frac{1}{1+e^{ktv_{ij}(t)}}\left(1 + \frac{d_{safedis}}{\left|\overrightarrow{d_{ij}(t)}\right|^{\tau}}\right) + \left\| \left[\frac{\partial cv_{ij}(t)}{\partial v_i}, \frac{\partial cv_{ij}(t)}{\partial v_j}, \frac{\partial cv_{ij}(t)}{\partial \theta_i}, \frac{\partial cv_{ij}(t)}{\partial \theta_j} \right]^T \right\|^{-1} & cv_{ij}(t) \geq 0 \end{cases} \tag{9}$$

3.1.2 Maritime traffic complexity calculation for multi-ship

Based on the complexity calculation method between pairwise ships presented in Section 2.1.1, this study further extends the approach to multi-ship interaction scenarios, constructing a maritime traffic complexity matrix A among multiple ships, as detailed in Equation (10):

$$A = \begin{bmatrix} a_{11}(t) & \cdots & a_{1j}(t) & \cdots & a_{1n}(t) \\ \vdots & \ddots & \cdots & \ddots & \vdots \\ a_{i1}(t) & \cdots & a_{ij}(t) & \cdots & a_{in}(t) \\ \vdots & \ddots & \cdots & \ddots & \vdots \\ a_{n1}(t) & \cdots & a_{nj}(t) & \cdots & a_{nn}(t) \end{bmatrix} \tag{10}$$

In the equation, n represents the total number of ships present in the waterway at time t.

The weight matrix of the maritime traffic complexity matrix A is calculated using Shannon entropy, which is objective and stable in multi-indicator weight calculation. The calculation results depend solely on the distribution characteristics of the indicator data and are unaffected by subjective factors, as shown in Equation (11). Finally, the overall complexity of each ship within the traffic situation at time t is obtained by performing the Hadamard product operation between the complexity matrix A and the weight matrix, as detailed in Equation (12):

$$w_{ij}(t) = -a_{ij}(t)\log a_{ij}(t) \tag{11}$$

$$c_{omplex}(t) = \sum_{j=1}^{n} a_{ij}(t) \odot w_{ij}(t) \tag{12}$$

In summary, this study proposes a maritime traffic complexity measurement model for multi-ship interaction scenarios based on ship-to-ship interaction mechanisms. This approach not only enhances the quantitative perception of potential collision risks in complex maritime environments but also provides a solid theoretical foundation for the subsequent construction and dynamic evolution modeling of the navigation energy field.

3.2 Navigation energy field model

In spatial data modeling, each data point within a given data object is typically influenced by surrounding data points. This influence relationship can be mathematically formalized through the use of potential functions. The potential function characterizes the intensity of the effect exerted by other data points on the target point, allowing the overall density of the data space to be represented as the superposition of the potential functions of all objects, thereby forming a complete density function model. On this basis, by defining appropriate forms of potential functions, it becomes possible to construct navigation energy field models tailored to specific contexts.

The navigation energy field is the core modeling framework proposed in this study. Its theoretical basis originates from the classic potential field theory, which was first widely applied in robot path planning and obstacle avoidance. In recent years, some Chinese scholars [11,29] have applied it to maritime traffic risk modeling. By treating ships as field sources, the researchers constructed a potential function model to describe the scope of risk influence, thereby enabling a spatial description of the navigation situation. Based on this, this study further develops the concept of navigation energy field, introducing maritime traffic complexity, multi-ship interaction relationships, and heterogeneous potential function overlay mechanisms, enabling the model to not only express the effect intensity brought about by relative distance, but also reflect the trend of traffic status on risk. Therefore, the navigation energy field not only possesses the spatial perception capabilities of traditional energy field models but also enhances the quantification and local response capabilities of risk identification, making it more suitable for navigation risk modeling and MoO switching decision-making in complex interactive scenarios.

Definition: A navigation energy field refers to a spatial continuum function model based on potential field theory, which is used to describe the intensity of potential risks and effects on a ship in a specific time and space location in a multi-ship interaction environment. By constructing directional potential functions and integrating ship motion states and complexity attributes, this model achieves a spatial visualization of potential collision risks, providing quantitative support for risk perception and MoO switching for MASS.

Existing studies predominantly use Gaussian functions or other radially symmetric functions as the basis for potential functions, typically generating navigation energy field models with circular shapes. While such models can capture the general trend of risk attenuation with increasing distance from the own ship, they fail to adequately account for the irregularity of the SD, particularly under multi-ship interactions or asymmetric traffic scenarios. Therefore, developing an asymmetric navigation energy field model that can comprehensively incorporate SD characteristics is of significant importance for improving the accuracy and adaptability of risk modeling.

In summary, the construction of an adaptive potential function should take into account the following factors:

1) The shape characteristics of the SD, and its spatial distribution effects on risk attenuation patterns. In particular, the risk should exhibit a sharp increase in the vicinity of the own ship's central area.

2) The crew's attention mechanisms under dense traffic conditions. During decision-making, ships should prioritize attention to nearby target ships, with distant targets receiving secondary consideration; therefore, the potential function should reflect this layered attention mechanism.

3) The interrelationships among multiple ships. In complex traffic scenarios, target ships are not independent of one another but form an interacting and mutually influencing system; thus, the potential function should be capable of capturing the spatial coupling effects among targets.

Based on this, the present study further develops a set of potential functions that meet the above requirements, with the design fully accounting for the interaction characteristics among ships. The model ensures perceptual capability for both nearby ships within 1.5 nm and more distant targets, thereby enabling dynamic capture of potential risks in both local and extended traffic environments, as detailed in Equation (13).

$$\begin{cases} y_1 = \dfrac{10c_{omplex}}{d^2} \\ y_2 = 50c_{omplex} * e^{-0.5d} \\ y_3 = \dfrac{15c_{omplex}}{d^3} \\ y_4 = \dfrac{30c_{omplex} * e^{-0.4}}{d^2} \\ y_5 = 5(\dfrac{1}{d^2} + 2e^{-0.4d}) \\ y_6 = 2c_{omplex}(e^{-0.05d^2} + e^{-2d^2}) \end{cases} \tag{13}$$

In the Equation, d represents the distance from the ship's center, and c_{omplex} denotes the maritime traffic complexity calculated from Equation (12), with a preset value of 3 in this context.

The constructed functions incorporate basic forms such as exponential, logarithmic, and Gaussian functions, which are further modified through transformation processing. The plots of each function are shown in Figure 4.

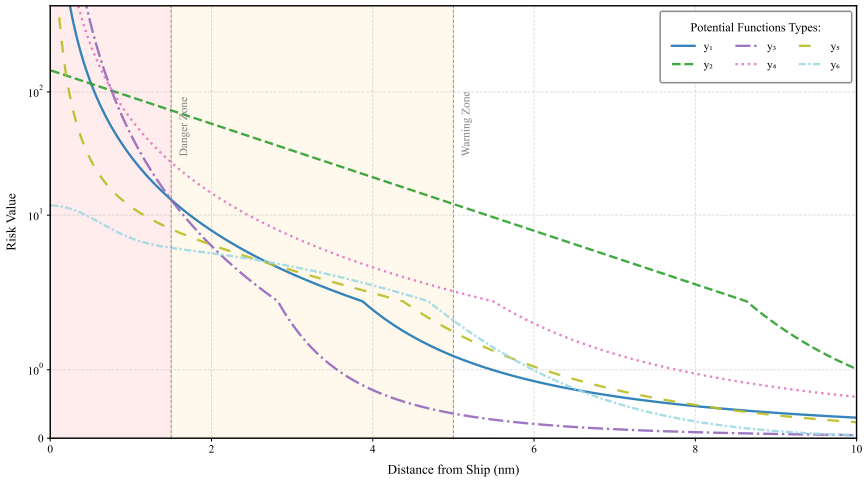

Fig. 4 Plots of the different potential functions

As shown in Figure 4, y_1, y_4 and y_5 exhibit steep growth within the danger zone but maintain relatively strong risk values even at long distances, making it difficult to effectively reflect the hierarchical nature of risk; the resulting risk region boundaries display unnaturally sharp features. Although y_2 demonstrates a certain degree of attenuation, it lacks clear risk transitions at medium and long distances, making it difficult to establish distinct boundary demarcations. On the other hand, y_3 exhibits overly rapid risk values decay across the entire range, which can result in insufficient responsiveness to near-field risks. In contrast, the Gaussian combination function corresponding to y_6 demonstrates the desired characteristics of rapid rise at close range and rapid decay at long distances, effectively emphasizing the risk intensity near obstacles while minimizing interference from distant targets in real-time collision-avoidance decision-making. Moreover, the y_6 curve exhibits smooth variation, offering good numerical stability and flexible parameter tuning, making it well-suited for application across different complexity scenarios.

To validate the robustness and stability of the constructed potential function in high-density traffic scenarios, this study systematically analyses the influence mechanisms of the c_{omplex} index and relative inter-ship distance on risk values. The sensitivity analysis of these two parameters is illustrated in Figure 5.

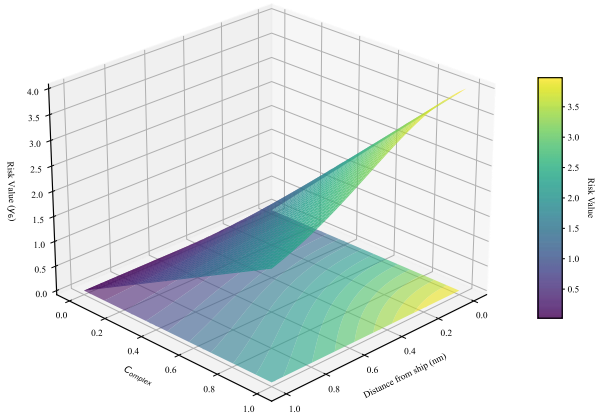

Fig. 5 Sensitivity analysis plot of the constructed potential function

In Figure 5, as the vessel separation distance decreases and the c_{omplex} parameter increases, the potential function captures the trend of non-linear growth in risk values. Moreover, the contribution of vessel separation distance to risk values is markedly greater than that of the c_{omplex} parameter. This aligns with actual navigation risks, where distance remains one of the primary factors influencing the risk of ship collisions. More significantly, even under extreme conditions where the inter-ship distance reaches its limit value, the risk value, while exhibiting an increasing trend, remains within reasonable bounds without exhibiting explosive growth. This demonstrates that the constructed potential function possesses sound numerical stability.

Therefore, the potential function ultimately adopted in this study is an improved Gaussian function. To additionally capture the influence of the number of ships within the scene on the navigation energy field, the final Gaussian function employed is defined as shown in Equation (14):

$$D = 2c_{omplex}(e^{-0.5d^2} + e^{-2d^2}) * \frac{1}{1 + n * g_{amma}} \tag{14}$$

In the Equation, D is the risk value of the navigation energy field, n is the number of ships detected in the navigation scenario. g_{amma} is a tuning parameter to avoid excessive influence of ship number fluctuations on the D.

The g_{amma} parameter in Equation (14) primarily serves to moderate the excessive influence of large fluctuations in number of ships on risk values. To validate the appropriateness of the g_{amma} parameter setting, this study conducts a comparative analysis of the trend in the potential function under different g_{amma} parameter values, as illustrated in Figure 6.

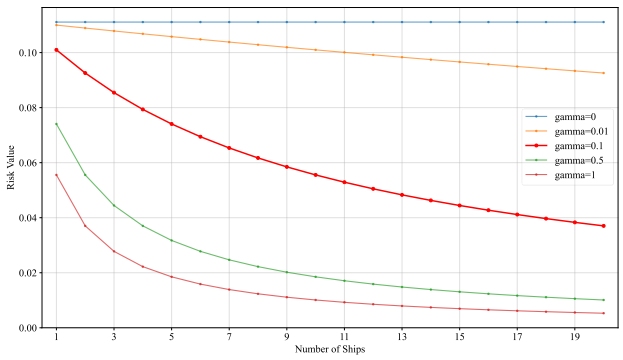

Fig.6 Sensitivity Analysis of the g_{amma} Parameter

Analysis indicates that as the number of ships increases, the g_{amma} parameter effectively suppresses the rate of growth in risk values without altering the overall trend in risk assessment, merely exerting a scaling effect. Notably, when number of ships exceed a certain threshold (7 vessels in Figure 6), the contribution of further increases to the risk value diminishes progressively. This phenomenon aligns with practical observations: mere numerical growth ceases to be the primary determinant of collision risk, with the complexity of the traffic situation becoming the more critical factor. Balancing sensitivity and stability in risk assessment, this study sets the gamma parameter at 0.1. This value effectively captures the influence of ship density on risk when number of ships are low, while preventing excessive risk estimates in high-density scenarios.

It should be pointed out that although this study uses a modelling method similar to potential function overlay in the construction of the navigation energy field, its mathematical expression is similar to that of traditional Kernel Density Estimation (KDE), but the two are fundamentally different: KDE aims to estimate probability density functions in static space, typically considering only spatial position variables and overlooking motion states and entity attributes. In contrast, the navigation energy field model constructed in this study is primarily used for modelling and identifying potential risks in dynamic navigation environments, comprehensively considering multi-dimensional dynamic characteristics such as the ship's speed, heading, length, and complexity. Furthermore, the kernel functions used in KDE are mostly symmetrical and smooth standard kernels, while the potential function designed in this study is a non-symmetrical Gaussian combination function, which has been adapted based on the PRSD model to better reflect the actual physical boundaries of ship collision avoidance behavior. Additionally, the output of KDE is a probability density value, whereas the navigation energy field output in this study directly reflects the risk overlap effects on the ship, supporting quantitative switching and risk classification for MoO. Therefore, although the model in this study draws inspiration from some of the ideas of KDE in terms of technology, it shows fundamental differences in terms of variable dimensions and function construction.

The navigation energy field generated using Equation (14) is illustrated in Figure 7, where the ship's heading is 124.1 degrees, speed is 11.3 knots, length overall is 199 meters, and the complexity value is set to 3.

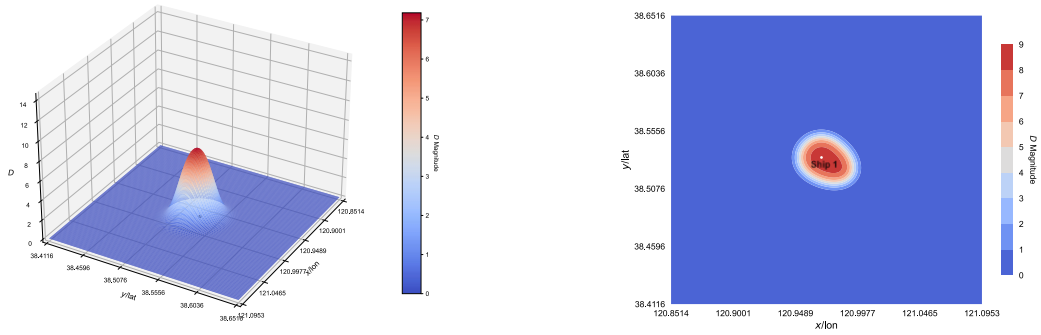

(a) (b)

Fig. 7 Schematic illustration of the navigation energy field generated by the improved gaussian function

In summary, this study incorporates maritime traffic complexity into the conventional potential field framework to construct a navigation energy field model that accounts for multi-ship interaction effects. The proposed model not only enhances the capability of the navigation energy field to characterize ship interactions and local risk evolution in high-density traffic areas but also improves its applicability and interpretability in complex navigation scenarios. By employing this method, MASS can actively perceive and dynamically respond to risk information, thereby providing a critical theoretical foundation and modeling basis for ensuring navigation safety in representative complex environments.

3.3 ALARP-based MoO zone definition

This study further introduces the ALARP principle to divide the navigation energy field into risk threshold regions, enhancing the adaptability and MoO switching capability of MASS under different risk

levels. The selection of confidence interval thresholds directly impacts the reliability and timeliness of MoO switching decisions. In Xin et al.'s research on modelling and assessing maritime traffic complexity, traffic complexity was categorized into four levels with corresponding thresholds of 51.76 %, 83.53 %, and 94.12 % [38]. These thresholds have been validated across multiple real-world waterways, demonstrating robust theoretical and practical foundations. Building upon Xin et al. findings, this study has made appropriate adjustments tailored to the specific requirements of operational mode switching. Consequently, risk values are categorized into four distinct zones: the Negligible Risk Zone (0–50 %), the ALARP Lower Risk Zone (50–70 %), the ALARP Upper Risk Zone (70–90 %), and the Intolerable Risk Zone (90–100 %). This adjustment primarily considers that appropriately lowering the threshold for high-risk levels enhances a vessel's sensitivity to risk changes, ensuring timely triggering of MoO switching. Furthermore, maintaining appropriate intervals between the three thresholds facilitates clear differentiation between different risk levels.

The Negligible Risk Zone corresponds to scenarios with low navigation safety risks, requiring no additional intervention, recommended MoO is Autonomous Mode (AM); the ALARP Zones emphasize reducing risk within reasonable and feasible limits, subdivided into lower and upper bounds to improve the precision of risk response, the recommended MoOs are Remote Mode (RM) and Onboard Crew Mode (OCM); the Intolerable Risk Zone represents high-risk scenarios that require immediate avoidance or emergency measures, recommended MoO is Emergency Mode (EM). This study has thoroughly verified the applicability and stability of this threshold division in preliminary experiments. The results show that under the current division conditions, the system can balance switching accuracy and frequency. Further narrowing or widening the threshold range will change the switching timing but will not significantly improve risk control effectiveness. Instead, it may introduce unnecessary frequent switching, weakening system stability. This classification provides a clear quantitative basis for MoO switching in complex environments, further enhancing the system's ability to identify and respond to risks in dynamic environments, as shown in Figure 8.

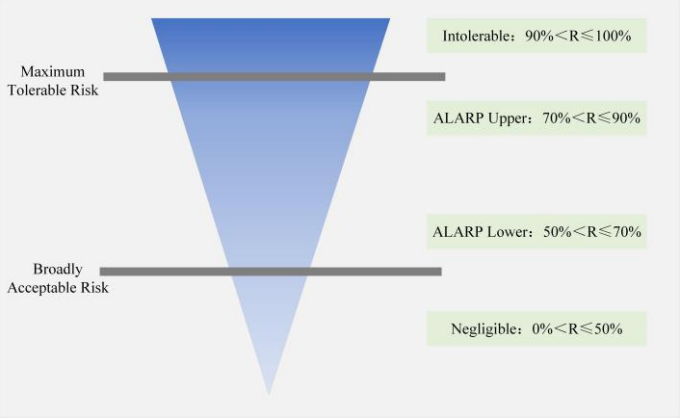

Fig. 8 Risk threshold classification of the navigation energy field

Considering that single-point risk values are highly susceptible to short-term fluctuations and often trigger frequent switching of MoO near risk level boundaries, this study introduces a risk assessment mechanism based on confidence intervals on the basis of the ALARP principle to improve the stability and robustness of system assessments. Specifically, the system uses a sliding window method to extract the most recent m risk value samples, as shown in Equation (15), and calculates the average risk value and sample standard deviation within the sliding window, as shown in Equations (16) and (17). The confidence interval at that point in time is then constructed based on the mean and standard deviation to measure the uncertainty of the risk situation, as shown in Equation (18):

$$R = \{D_{t-m+1}, D_{t-m+2}, \cdots, D_t\} \tag{15}$$

$$\bar{R} = \frac{1}{m}\sum_{i=1}^{m} D_i \tag{16}$$

$$s = \sqrt{\frac{1}{m-1}\sum_{i=1}^{m}(D_i - \bar{R})^2} \tag{17}$$

$$CI = [\bar{R} - z_{\alpha/2} \cdot \frac{s}{\sqrt{m}}, \bar{R} + z_{\alpha/2} \cdot \frac{s}{\sqrt{m}}] \tag{18}$$

In the Equation, D_t represents the risk value of the navigation energy field at time t calculated according to Equation (14); m is the number of risk value samples in the sliding window. According to the research by Liu et al. [39], the maritime traffic situation may significantly change approximately every 3 minutes. Therefore, this study sets m as 3 to ensure the timeliness and representativeness of the risk trend judgment; R is the current sliding window interval; $\bar{R}$ is the average risk value within the window; s is the standard deviation of the samples; $z_{\alpha/2}$ is the confidence coefficient, set to 1.96 in this study, corresponding to a 95 % confidence level; CI is the confidence interval of the sliding window.

To validate the appropriateness of selecting m and CI parameters during mode switching, this study conducted a sensitivity analysis. The analysis was based on data from overtaking scenarios, primarily because these scenarios exhibit prolonged duration and relatively stable risk value fluctuations, thereby fully reflecting the impact of parameter settings on switching behavior. Details are illustrated in Figure 9.

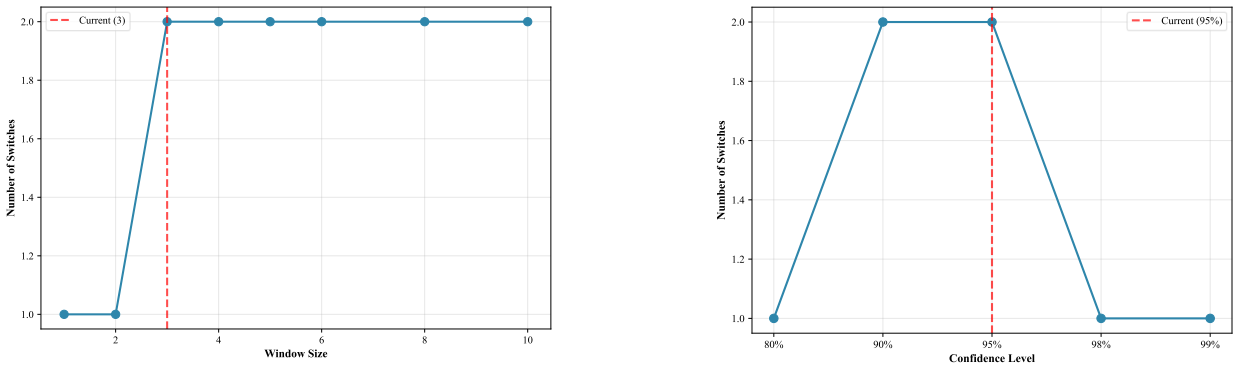

(a) (b)

Fig.9 Sensitivity analysis of parameters m and CI

As illustrated in Figure 9(a), when m is set to 3, the system effectively captures the trend in risk values. While increasing the window size beyond this value maintains the same switching frequency, it leads to a widening of the confidence interval, introducing unnecessary uncertainty that may delay the response time of switching decisions. Therefore, setting m to 3 achieves a favorable balance between sensitivity and stability. As illustrated in Figure 9(b), the 95 % confidence level not only aligns with standard statistical conventions but also maintains a favorable equilibrium in terms of stability. While lower confidence levels may yield faster response times, they risk triggering excessive switching frequency. Conversely, higher confidence levels may delay critical switching opportunities, thereby increasing navigational safety hazards for vessels.

Considering that the risk value of the navigation energy field usually varies continuously and there are no significant changes, this study does not consider MoO switching between levels and only focuses on switching between adjacent levels. To avoid frequent MoO switching due to risk value fluctuations, this study designs a multi-stage MoO switching strategy based on confidence interval risk judgement logic: When the confidence interval is completely within a certain ALARP risk level range, the system recommends the MoO recommended for that risk level range as the current recommended MoO. If the confidence interval spans two or more risk ranges, the system calculates the coverage ratio in each range and takes the MoO corresponding to the range with the largest ratio as the recommended MoO. If multiple intervals have the same coverage ratio, the MoO corresponding to the risk level with the higher risk level is selected to ensure the priority of the system's safety response. At the same time, to prevent the MoO from switching frequently near the risk level boundary, the system adopts a delay mechanism, which only triggers a switch when the recommended

MoO is inconsistent with the current MoO and the recommended MoO remains consistent for two consecutive times, avoiding mode switching caused by short-term risk fluctuations, as shown in Figure 10.

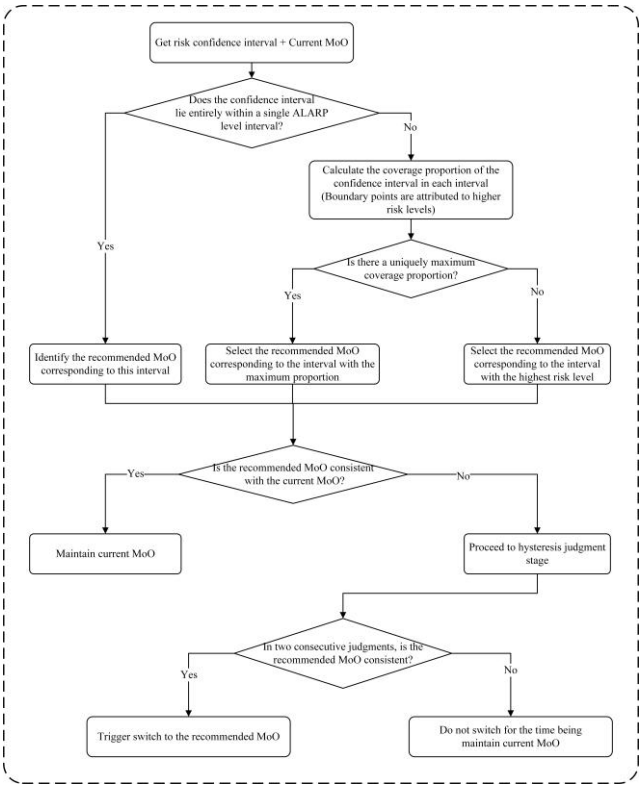

Fig. 10 Multi-stage MoO switching strategy based on confidence interval risk judgement logic

To sum up, this study provides a systematic discussion in Section 2 on the quantification of maritime traffic complexity, the construction of the navigation energy field, and the division of risk thresholds. By introducing multidimensional complexity indicators, the dynamic interaction relationships between ships are thoroughly considered, providing a solid data and structural foundation for navigation energy field. The design of the potential function effectively enhances the model's capability to capture the risk evolution trends in multi-ship encounter scenarios. Finally, by incorporating the ALARP principle, a classification of navigation risk levels is established, laying the theoretical foundation for the subsequent safe and efficient MoO switching of MASS in complex dynamic environments.

4. Case study

To validate the effectiveness and advanced features of the proposed model, this study designed two types of experimental scenarios: first, a simulation environment and second, a real navigation environment, to enhance the reliability of the research conclusions. In the simulation environment, three typical scenarios from COLREGs—overtaking, head-on, and crossing situations-were constructed to evaluate the model's adaptability. In the real environment experiment, a typical section of the Laotieshan Channel in the Bohai Sea was selected as the research object to further verify the model's applicability in actual complex navigation environments.

The validation work was conducted in an efficient Python 3.10 environment, using custom scripts developed and executed within the PyCharm (Version 2022) integrated development environment. And the model was validated on a high-performance computer equipped with an Intel Core i5-12500H processor, an NVIDIA RTX 2050 GPU, and 16 GB of RAM.

4.1 Simulation environment experiment

To systematically evaluate the applicability and performance of the proposed model in various typical navigation situations, this study first verifies the feasibility of the model in a constructed simulation environment. The simulation environment, with the advantages of strong controllability, adjustable variables, and repeatable results, is suitable for verifying and comparing the core mechanisms of the model. To comprehensively evaluate the performance and applicability of the proposed model, this study further introduces the maritime traffic complexity model proposed by Wen et al. [21] as a comparison. Comparative experiments are conducted under the same initial conditions and traffic scenarios to analyze the performance advantages of the proposed model in typical navigation scenarios.

4.1.1 Overtaking situation

The initial information of the two ships in the overtaking situation is shown in Table 1. Assuming that Ship A is the own ship and Ship B is the target ship, all evaluation indexes are calculated based on the influence of Ship B on Ship A. Figure 11(a) shows the risk values and their changes calculated by the model proposed in this study, marked in red and represented by curves, while the blue lines correspond to the calculation results of the comparison model. Figure 11(b) shows the changes in various indicators in the model proposed in this study.

Table 1 Initial information of ships in overtaking

	Initial Location (N, E)	Course (°)	Speed (knot)	Length (m)
Ship A	(38°24′0.00″,120°58′8.40″)	0	10	240
Ship B	(38°21′0.00″,120°58′8.40″)	0	14	240

As shown in Figure 11(a), Ship A is the overtaken ship and Ship B is the overtaking ship. As time proceeds, the relative distance between the two ships continues to decrease, and the influence of Ship B on Ship A gradually increases, causing the corresponding risk value to rise significantly. Both the proposed model and the comparison model effectively capture the trend of risk value changes for Ship A. However, the comparison model exhibits a more pronounced growth pattern throughout the risk value change process, with a wider range of risk values, and a significant increase only occurring in the later stages of the voyage, indicating a certain degree of response lag in the early stages of risk evolution; In contrast, the proposed model demonstrates higher risk sensitivity and discrimination during the vessel approach process, enabling earlier identification of potential conflict risks and facilitating timely decision-making. Based on the switching logic proposed herein, within the constructed overtaking situation, Ship B underwent two operational mode switches. The first occurred at time step 15, when the relative distance between the vessels gradually diminished and collision risk markedly increased. At this juncture, a switch from AM to RM is recommended. Subsequently, as the vessel risk continues to escalate beyond a higher threshold, a further transition to OCM is advised at time step 23 to ensure navigational safety. In contrast, the comparison model, due to its slower risk progression, fails to detect the critical threshold for a timely switch and consequently misses the required transition point. This demonstrates that the proposed approach exhibits superior sensitivity and early warning capabilities during periods of rapid risk evolution.

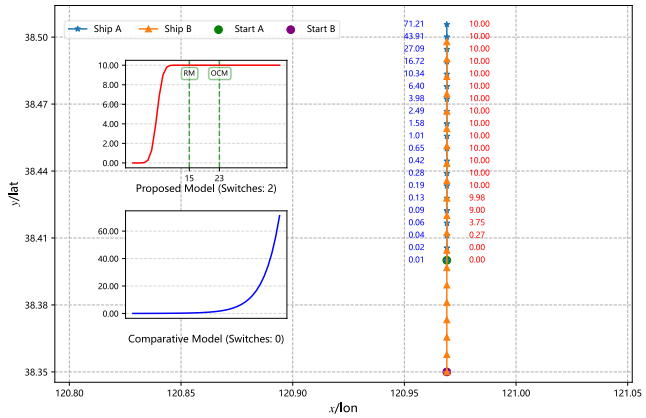

(a)

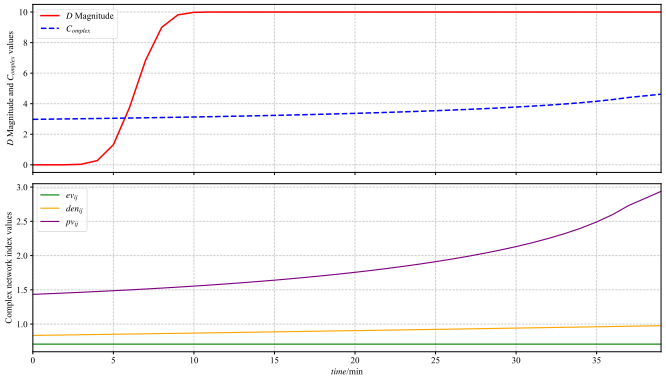

(b)

Fig. 11 Overtaking situation: ship trajectory and risk value variations

Figure 11(b) further illustrates the temporal evolution of the navigation energy field risk value D and the complexity value $c_{complex}$ of Ship A under overtaking situations in the model proposed (upper figure), as well as the trends of the three complex network index values $den_{ij}(t)$, $pv_{ij}(t)$, and $ev_{ij}(t)$. As shown in the upper part of Figure 11(b), the D value is initially 0, indicating that the two ships have not yet established significant interaction relationships. It then rises rapidly after the 7th minute and tends toward its maximum value after the 10th minute. This abrupt change reflects the rapid increase in interaction intensity between the two ships during the overtaking situation, leading to a significant increase in risk perception. At the same time, the $c_{complex}$ increases steadily over time, exhibiting good continuity and dynamic response characteristics. As can be further observed in the lower part of Figure 11(b), Among the three complex network index values, $pv_{ij}(t)$ dominates and shows a continuous increasing trend, indicating that the collision avoidance manoeuvring space of the ships is continuously shrinking and the potential collision is intensifying during the overtaking, while $den_{ij}(t)$ and $ev_{ij}(t)$ show a slow upward trend, reflecting the gradual increase in the density of nearby ships and the difficulty of local traffic mitigation.

4.1.2 Head-on situation

The initial information of the two ships in the head-on situation is shown in Table 2. Assuming that Ship A is the own ship and Ship B is the target ship, all evaluation indexes are calculated based on the influence of Ship B on Ship A. Figure 12(a) shows the risk values and their changes calculated by the model proposed in this study, marked in red and represented by curves, while the blue lines correspond to the calculation results of the comparison model. Figure 12(b) shows the changes in various indicators in the model proposed in this study.

Table 2 Initial information of ships in head-on situation

	Initial Location (N, E)	Course (°)	Speed (knot)	Length (m)
Ship A	(38°21′0.00″,120°58′8.40″)	180	10	240
Ship B	(38°6′0.00″,120°58′8.40″)	0	14	240

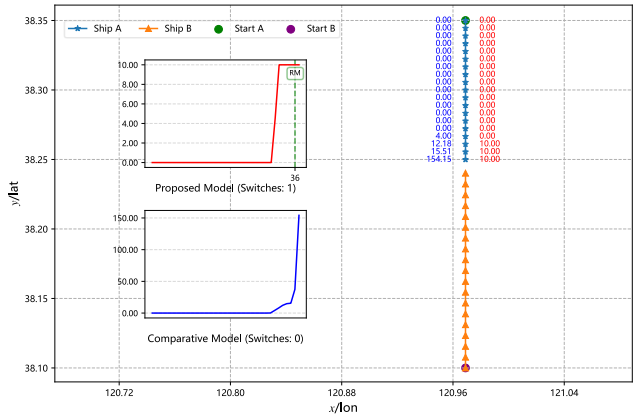

(a)

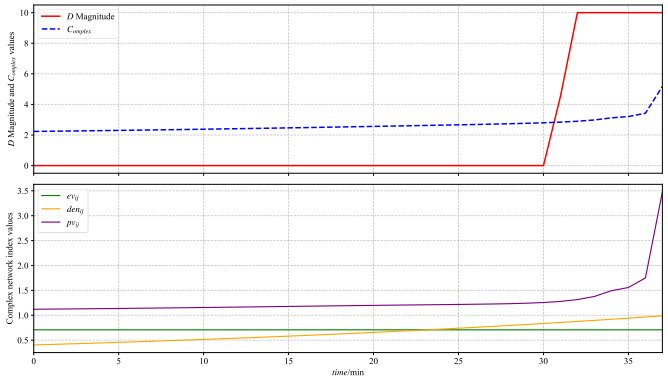

(b)

Fig. 12 Head-on situation: ship trajectory and risk value variations

Figure 12(a) shows the trajectories of two ships in a head-on situation and the changes in their risk values. As can be seen from the comparison in the figure, although both models can capture the upward trend in risk values, they exhibit different response characteristics. The comparison model exhibits a certain degree of continuity in risk value changes but with significant fluctuations, reaching a risk peak toward the end. In contrast, the model proposed in this paper responds earlier to risk changes, showing a noticeable increase in risk values during the initial phase, followed by a stabilization of risk values, indicating a more sensitive perception of potential risks. Owing to the more pronounced fluctuations in vessel-to-vessel risks within the Head-on situation, the proposed model detected only one mode switch at time step 36, whereas the comparative model still failed to identify the transition point.

As can be seen from the upper part of Figure 12(b), the risk value changes more rapidly in a head-on situation than in an overtaking situation. During the initial 30 minutes, the two ships did not form a significant interaction relationship. In this stage, the D value of Ship A, as calculated by the model proposed in this paper, remained basically at 0. However, starting from the 30th minute, under the influence of Ship B, the D value rapidly increased, reflecting a rapid increase in the collision risk between the two ships. At the same time, c_{omplex} also showed a steady increasing trend. Although the change was relatively moderate, it still effectively responded to the changes in the risk situation. Further analysis of Figure 12(b) below reveals that the three complexity index values $den_{ij}(t)$, $pv_{ij}(t)$, and $ev_{ij}(t)$ show distinct trends, with $pv_{ij}(t)$ exhibiting the most

significant changes, indicating that the proximity between the two ships underwent drastic changes during this time period.

4.1.3 Crossing situation

The initial information of the two ships in the crossing situation is shown in Table 3. Assuming that Ship A is the own ship and Ship B is the target ship, all evaluation indexes are calculated based on the influence of Ship B on Ship A. Figure 13(a) shows the risk values and their changes calculated by the model proposed in this study, marked in red and represented by curves, while the blue lines correspond to the calculation results of the comparison model. Figure 13(b) shows the changes in various indicators in the model proposed in this study.

Table 3 Initial information of ships in crossing situation

	Initial Location (N, E)	Course (°)	Speed (knot)	Length (m)
Ship A	(38°21′0.00″,120°53′24.00″)	0	10	240
Ship B	(38°24′0.00″,120°58′8.40″)	270	14	240

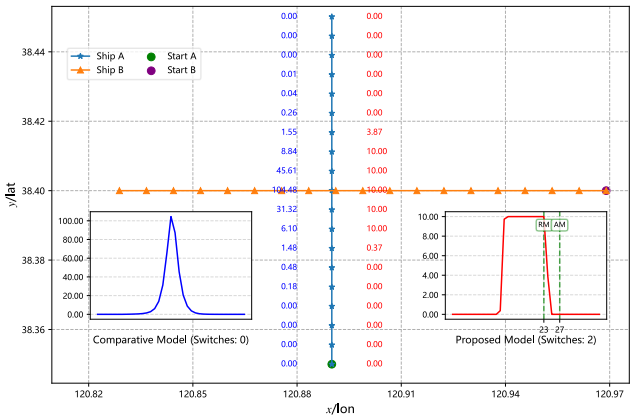

(a)

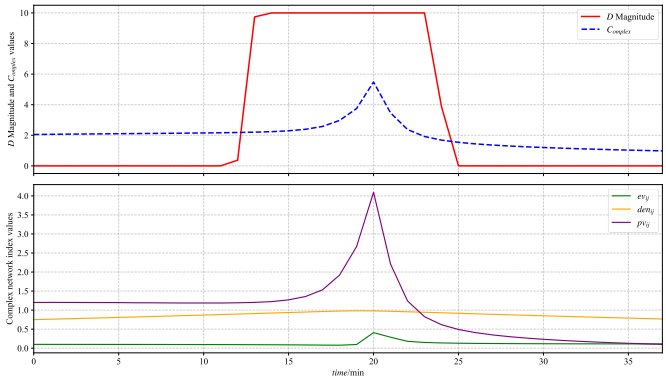

(b)

Fig. 13 Crossing situation: ship trajectory and risk value variations

Figure 13(a) shows the trajectories of two ships during their crossing and the changes in their risk values. Both the proposed model and the comparison model accurately reflect the overall trend of risk value changes, i.e., the risk value exhibits the typical characteristic of first increasing and then decreasing during the ship encounter. However, the two models show significant differences in their detailed performance. The comparison model exhibits significant fluctuations in risk value changes, with peaks occurring rapidly but lasting for a short duration, indicating greater sensitivity to instantaneous changes. In contrast, the proposed model not only captures the main trend of risk values but also maintains a prolonged duration at risk peaks,

demonstrating strong risk capture capabilities. In the crossing situation, this study similarly detected the necessity for two operational mode switches. The first transition was recommended at time step 23 to switch to RM. Due to the rapid evolution of risk, a further transition to OCM was advised at time step 27. In contrast, the comparison model failed to trigger any operational mode switches as it did not capture the sustained high-risk state.

As can be seen from the upper part of Figure 13(b), under the influence of ship B, the D value of ship A first increases and then decreases, reflecting the typical risk evolution characteristics of the two ships during the approach and separation processes. The $c_{complex}$ also shows a similar trend, indicating that this index effectively captures the dynamic changes in interaction risk. Further analysis of the lower panel of Figure 13(b) shows that all three complexity index values peaked around the 20th minute and then gradually decreased, indicating that the two ships were at their closest relative distance and had the strongest interaction at that time, marking the high-risk period of the crossing situation.

Analysis of the three typical situations above demonstrates that the model proposed in this study exhibits certain advantages in risk monitoring and mode switching. It can promptly capture trends in risk changes between vessels, enabling early warning and thereby enhancing the safety of vessel navigation.

4.2 Real environment experiment

This study also selected a typical navigation segment of the Laotiushan Channel in the Bohai Sea as a real-world environmental research subject. Given the relatively fixed shipping routes in the Bohai Sea and the limited variation in ship tracks within the study area, this region is highly representative. To support model validation, AIS trajectory data from all vessels equipped with AIS devices in the Bohai Sea on June 1, 2023, were collected and analyzed, thereby defining the scope of the study area, as shown in Figure 14.

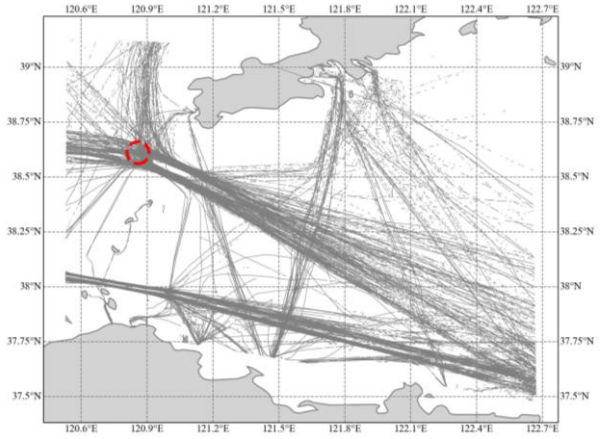

Fig. 14 Ship trajectories in the Bohai Sea on June 1, 2023

As shown in Figure 14, there are several areas where ship trajectories intersect in the Bohai Sea, with the Laotiushan Channel Traffic Separation Scheme (TSS) Precautionary Area, highlighted by the red box, being particularly prominent. This area is located at a key node on an important shipping route in the Bohai Sea, where ships frequently enter and exit, resulting in high traffic flow. Moreover, a significant number of vessels navigate in opposite directions, creating potential for traffic conflicts and collision risks. Given its high research value and representativeness [40], this area is selected as the research case for validating and applying the proposed traffic complexity measurement method and navigation energy field model.

As this study primarily relies on AIS data, issues such as irregular transmission intervals, signal interference, and packet loss necessitate data pre-processing prior to analysis. This ensures data accuracy and stability. The pre-processing workflow encompasses data cleansing to eliminate duplicate records, position discontinuities, and invalid coordinates. Subsequently, cubic spline interpolation is applied to resample all vessel tracks to a consistent time interval, addressing irregular sampling while preserving trajectory smoothness. Thereafter, a moving average filter is employed to mitigate positional noise and heading jitter. The complete pre-processing workflow is illustrated in Figure 15.

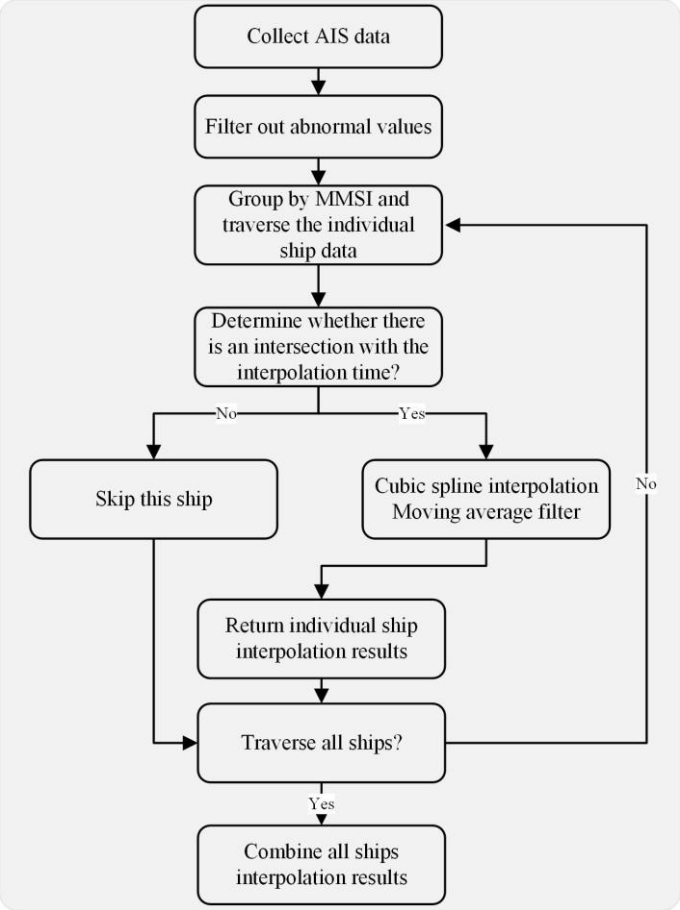

Fig.15 AIS data pre-processing flowchart

4.2.1 Data selection

This study selected the AIS data of ships at 18:20 on June 1, 2023, as the case validation data for the maritime traffic complexity and navigation energy field model. The AIS information and distribution map of the ships at this time are shown in Table 4 and Figure 16, respectively.

Table 4 AIS Data of Ships in the Laotieshan Precautionary Area (18:20, June 1, 2023).

	Latitude (degree)	Longitude (degree)	Heading (degree)	Speed (knot)	Length (m)
Ship 1	38.53354	120.96937	124.1	11.3	199
Ship 2	38.5783	120.9017	145.6	11.9	161
Ship 3	38.58863	120.86549	139.8	12.6	185
Ship 4	38.53128	120.91338	114	11.2	172
Ship 5	38.5005	121.00227	123.2	11.7	85
Ship 6	38.5663	120.91932	130.8	12	150
Ship 7	38.63302	120.90712	299.9	9.4	157
Ship 8	38.60594	120.84565	134.2	10.3	199
Ship 9	38.72795	120.93141	338.2	7.9	126

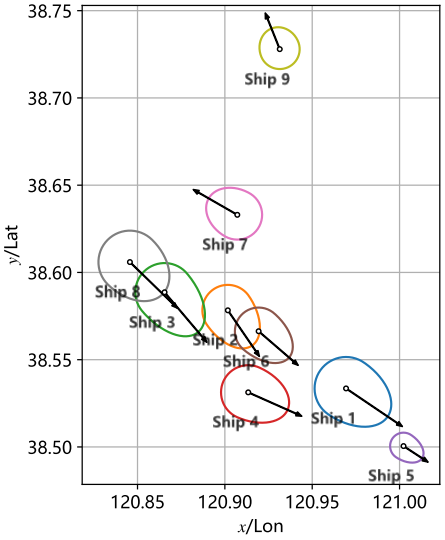

Fig. 16 Ship Distribution in the Laotieshan Precautionary Area (18:20, June 1, 2023)

Figure 16 shows the ship distribution in the Laotieshan Precautionary Area at 18:20 on June 1, 2023. The different colored ellipses represent the PRSDs (calculated using Equation (5)), and the black arrows indicate the heading and speed of the ships. As can be seen from Figure 16, ship distribution in this area is relatively dense, with localized crossing risks. In particular, the interactions between Ship2, Ship6, Ship4, and their nearby vessels appear more urgent and critical.

4.2.2 Maritime traffic complexity calculation

Using the maritime traffic complexity measurement model developed in Section 2.1, the complexity levels of each ship within the study area were quantitatively calculated, and the results are shown in Figure 17.

As observed from the figure, Ship4 and Ship7 exhibit the highest complexity values, at 4.12 and 4.03 respectively, indicating that these two ships are currently situated in the most complex traffic situations. Further analysis based on the ship distribution in Figure 17 reveals that Ship4 is involved in crossing encounters with Ship6 and Ship2, while simultaneously converging with multiple other ships, thus forming a local multi-directional interference zone that significantly increases its complexity. Although Ship7 does not display clear head-on or overtaking interactions with surrounding vessels, its heading differs markedly from nearby ships, creating a relatively high potential collision risk and thus a high complexity level.

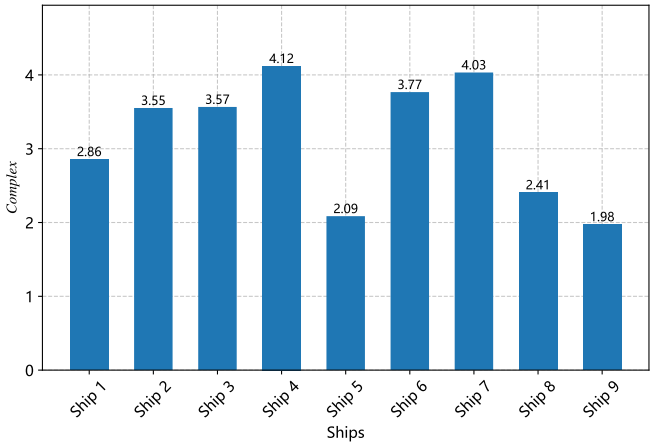

Fig. 17 Calculation results of maritime traffic complexity in the Laotieshan Precautionary Area (18:20, June 1, 2023)

In contrast, Ship5 and Ship9 have the lowest complexity values, at 2.09 and 1.98 respectively, indicating that these ships face minimal interference in the current traffic environment. Their surrounding vessel density is low, and the heading relationships are relatively stable, resulting in a clearer and safer traffic situation.

This case study validates the effectiveness of the complexity model in identifying key vessels and high-risk zones, providing a solid foundation for the subsequent construction of the navigation energy field and navigation risk assessment.

4.2.3 Navigation energy field calculation

After calculating the maritime traffic complexity values of each ship, a ship-based potential source navigation energy field model is constructed based on the principles of field theory. The spatial modeling of the study area is achieved through the potential function, and the three-dimensional and two-dimensional ship navigation energy field maps are generated, as shown in Figures 18 and 19.

From the figures, it is evident that there is a distinct spatial correlation between ship distribution and the navigation energy field. For instance, the concentration of ships such as Ship2, Ship3, Ship4, Ship6, and Ship8 leads to a significant overlap of their surrounding energy fields, creating multiple high-risk peak regions. These areas are prominently shown as "uplifts" in Figure 18 and appear as red high-value regions in Figure 19, reflecting the potential collision and conflict risks in the complex traffic environment. In contrast, ships located in the peripheral regions, such as Ship1, Ship5, and Ship9, are relatively isolated, with no dense interference from other ships. Consequently, their navigation energy field distributions are independent, although the field strengths vary due to the differing navigation states of each ship.

Further analysis, incorporating the ship distribution and heading information from Figure 16, reveals that in addition to position concentration, the relative motion relationships between ships also play a crucial role in navigation energy field overlap. For example, Ship3 and Ship8 exhibit a clear crossing tendency, which significantly enhances the overlapping region of their navigation energy fields. This spatial coupling effect of risk is reflected in the steeper variations in field values in the three-dimensional plot. Additionally, Figure 19 provides a two-dimensional view of the energy diffusion and overlap distribution of each ship, which facilitates the rapid identification of potential high-risk areas by MASS.

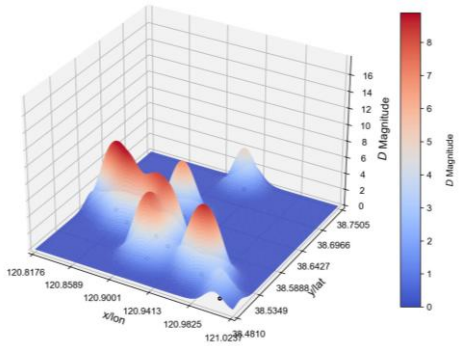

Fig. 18 The three-dimensional navigation energy field in the Laotieshan Precautionary Area (18:20, June 1, 2023)

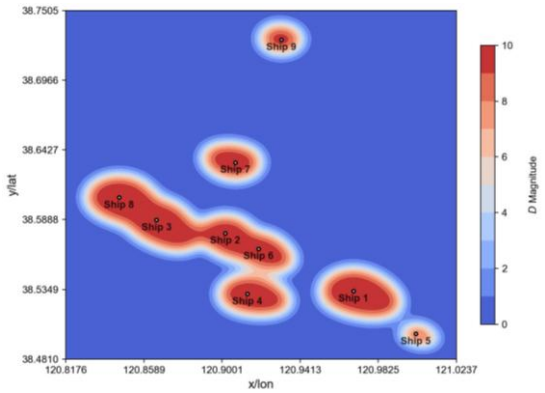

Fig. 19 The two-dimensional navigation energy field in the Laotieshan Precautionary Area (18:20, June 1, 2023)

Due to the rare occurrence of highly urgent situations in maritime traffic environments, this study simulates a trajectory based on the results calculated from Figures 18 and 19, specifically in the traffic scenario

shown in Figure 19, to evaluate the risk level of the trajectory within the current navigation energy field, as shown in Figure 20. The trajectory passes through multiple navigation energy field overlap areas, with a noticeable increase in risk values, especially when passing through the high-risk zone between Ship6 and Ship2. The maximum risk value reaches 9.87, indicating that this area has a high potential for collision risks. In contrast, when the trajectory passes through edge areas such as near Ship1 and Ship3, the risk values remain relatively low, and the overall field strength changes smoothly. This experiment validates the ability of the constructed potential field function to respond to navigation risks in complex traffic situations and demonstrates that the method presented in this study can effectively depict the risk evolution process of dynamic trajectories within specific maritime environments.

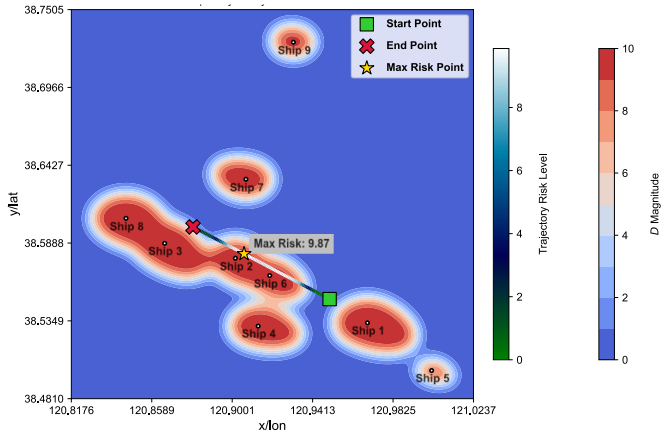

Fig. 20 Navigation energy field of simulated trajectory in specific situation

By introducing the ALARP principle, the navigation risk values of simulated trajectory are categorized into four levels to more intuitively reflect the distribution of the trajectory across different risk zones. Specifically, the computed risk values are classified into four intervals: 0–50 %, 50–70 %, 70–90 %, and 90–100 %, corresponding to the Negligible Risk Zone (Zone Four), the ALARP Lower Risk Zone (Zone Three), the ALARP Upper Risk Zone (Zone Two), and the Intolerable Risk Zone (Zone One), respectively. As illustrated in Figure 21, the trajectory predominantly resides within the low-risk segments (Zone Four and Zone Three); however, when traversing the high-risk area between Ship6 and Ship2, portions of the trajectory enter the orange and red zones, indicating elevated safety risks.

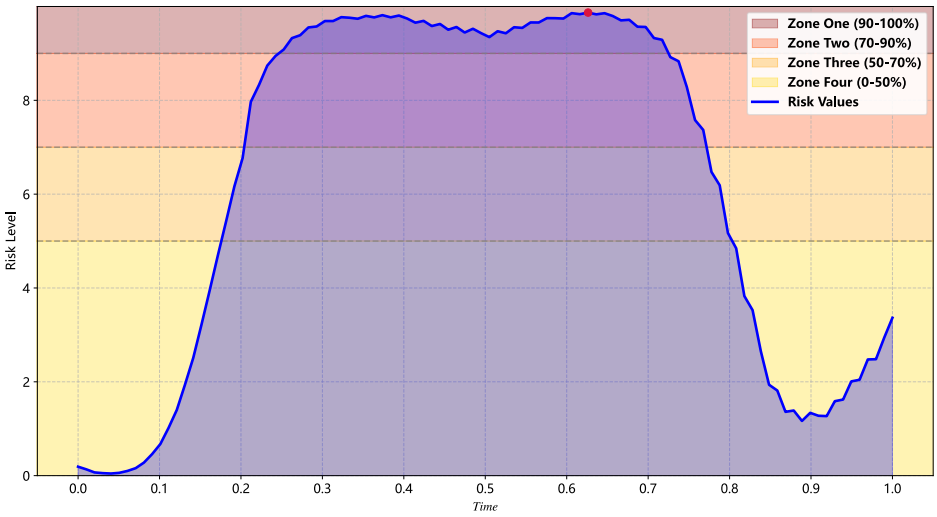

Fig. 21 Simulated trajectory navigation energy field risk values based on ALARP

4.2.4 Validation with real navigation case study

To validate the applicability and engineering feasibility of the proposed navigation energy field model incorporating multi-ship interaction characteristics in real navigation environments, this section selects the

historical AIS track of a target ship A in the Bohai Sea as the research subject. The ship departed from the port, passed through the Precautionary Area of the Laotieshan Channel, and entered open waters, covering typical navigation scenarios such as port entry/exit, narrow waterways, and open seas. The historical track of this vessel is shown in Figure 22.

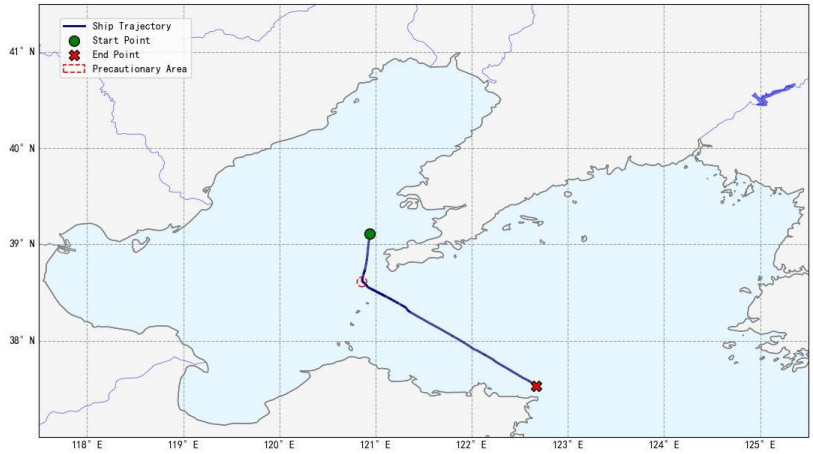

Fig. 22 Track chart of target ship A in the Bohai Sea from 2 to 3 June 2023

The study focuses on the track of target ship A in the Bohai Sea. Due to limitations in the availability of AIS data, the entire port entry and exit process could not be covered, and only the navigation data of the ship from port exit through the Laotie Shan Precautionary Area to open waters was obtained. If the AIS data extraction radius is too small, there will be insufficient information available; if it is too large, it will introduce information redundancy and increase the computational burden. This paper comprehensively considers information integrity and computational efficiency, draws on the idea of collision avoidance stage division, selects the dynamic information of all surrounding ships within a 12 nm radius of the target ship, and dynamically calculates the risk level of the target ship A's situation at each moment at 5 second intervals. Subsequently, based on the ALARP principle, the risk levels of each scenario at each time point are classified into four different risk zones, as shown in Figure 23.

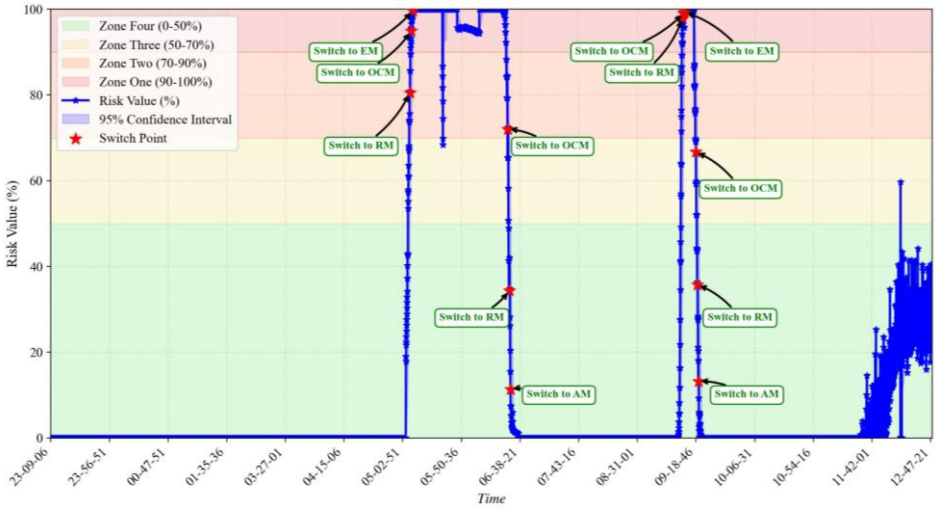

Fig. 23 ALARP-based target ship A risk value change chart

As can be seen from Figure 23, target ship A experienced a total of 12 MoO switches during this voyage, indicating that the risk level during this voyage showed significant time-varying characteristics. Overall, the ship's risk values remained at relatively low levels for most of the voyage, indicating that it was in a relatively safe state during the entire operation. However, during certain specific time periods, the fluctuations in risk values increased significantly, with multiple high-risk peaks occurring, accompanied by multiple mode switches. For example, between 5:02:51 and 6:38:21, the ship's risk value rose to Zone One, entering a high-

risk area, and triggered multiple MoO mode switches. It is worth noting that although the risk value declined after reaching extremely high levels during this period, the switching conditions were set to require two consecutive determinations within the confidence interval, and the switching trigger conditions were not met in the short term, thus no new MoO switching was triggered, enhancing the system's robustness; Another critical time period occurred around 9:18:46, when the ship again experienced multiple MoO switches. Although the risk value briefly reached the switching threshold during this period, it fluctuated for a short time and quickly fell back. However, the proposed model was still able to effectively capture the necessity of the MoO switch, demonstrating its sensitivity in responding to rapidly changing risks. In addition, at around 11:42:01, although the risk value of the ship fluctuated to a certain extent again, due to the strict confidence interval constraints set by the system, the risk value did not reach the criteria for mode switching and the original mode was maintained. This shows that the current mode switching strategy can still effectively avoid unnecessary mode switching in the face of certain risk fluctuations, further improving the overall reliability of the system.

To further validate the applicability and superiority of the proposed model at a more microscopic level, this study selects another target ship B operating in the Bohai Sea as the research subject, using one of its voyages in 2023 as the analysis scenario to investigate the dynamic changes in risk values under real-world navigation situations. The study area is defined as a circular region with a radius of 5 nm, centered on the Precautionary Area of the Laotieshan Channel. The research period spans the entire duration from the target ship B's entry into the study area to its exit (from 11:00:17 to 11:47:47 on June 2, 2023). The navigation trajectory of the target ship B during this period is shown in Figure 24.

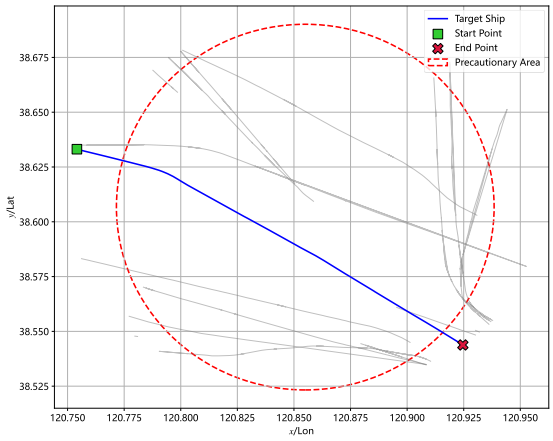

Fig. 24 Target ship B entering and departing the Laotieshan Precautionary Area trajectory

Fig. 25 Visualization of target ship B risk values based on ALARP

Starting from the moment the target ship B entered the designated area, AIS data for all vessels within a 5 nm radius were collected. The risk level of the target ship was dynamically calculated at 5s intervals for

each time point within the scene. The ALARP principle was similarly applied to categorize the scene risk at each time point into four graded zones. The specific results are shown in Figure 25. Since no substantial risk correlation had formed around the target ship during its initial entry into the Precautionary Area (from 11:00 to 11:17), the AIS data from 11:17:30 to 11:47:25 on June 2, 2023, were selected as the representative period for detailed analysis.

Figure 25 illustrates the dynamic variation trend of the target ship B's risk value throughout the entire navigation process, where the horizontal axis represents each navigational scenario divided by time, and the vertical axis denotes the corresponding risk values. The background color band divides the risk into four intervals, each corresponding to a different recommended MoO. The blue curve represents the risk value, and its trend intuitively reflects the dynamic changes in the risk level. The blue semi-transparent area represents the 95 % confidence interval of the risk value, which reflects the reliability and uncertainty of the risk assessment results. The red asterisk marks the MoO switching point.

As can be seen from Figure 25, during the initial phase of the target ship B's entry into the study area, its risk value was low and remained in Zone Four, indicating that there were few surrounding ships during this period and the navigation environment was relatively safe. At the same time, due to the small fluctuations in the risk value and the narrow confidence interval, the risk assessment results were highly stable. However, starting at 11:27:15, the target ship's risk value gradually increased, and the confidence interval began to show trailing shadows, indicating increased risk uncertainty. At 11:33:35, after two confidence interval assessments, it was recommended to switch MoO to RM, reflecting that the surrounding traffic situation was becoming more complex at this stage, with the possibility of high-risk interactions such as ship encounters, convergence, or overtaking. Subsequently, at 11:34:45, based on the MoO switching logic, it was further recommended to switch to OCM; by 11:35:45, the risk value continued to rise and stabilized in Zone One, prompting the system to recommend switching to EM, indicating that this phase had entered a high-risk state and requiring special attention.

To further investigate the specific dynamics of the target ship B's risk during this critical period, the continuous scenarios from 11:32:00 to 11:37:00 were extracted and analyzed in detail. The corresponding results are presented in Figure 26, where the red-marked SD in the ship distribution diagram denotes the target ship B.

As shown in Figure 26, between 11:32:00 and 11:37:00, the target ship B gradually entered the SD of the other ship and formed a clear convergence pattern. As the relative distance continued to decrease, the potential collision risk increased significantly.

From the evolution of the navigation energy field risk value, by around 11:34:00, the target ship B's risk value had risen to 50 % of the scene set threshold, indicating that it had entered the 'higher risk' phase. As shown in Figure 25, around 11:34:45, after two consecutive confidence interval assessments, the system recommended switching the target ship's operating mode to OCM to enhance situational awareness and improve emergency response efficiency, thereby ensuring navigational safety.

By approximately 11:35:00, the minimum distance between the target ship B and other vessels further decreased, and the risk value rose to 90 % of the set threshold, entering the 'high risk' zone. Subsequently, the system again made consecutive determinations through the confidence interval mechanism and recommended that the target ship B's operating mode be further switched to EM in order to promptly initiate the preset emergency response procedures or avoidance strategies and minimize the potential collision risk.

The above process demonstrates that the MoO dynamic adaptation mechanism based on traffic situation awareness and risk quantification can effectively enhance the navigational safety of ships in complex interaction scenarios, verifying the applicability and practical value of the maritime traffic complexity assessment and navigation energy field modelling methods proposed in this paper in actual navigational environments.

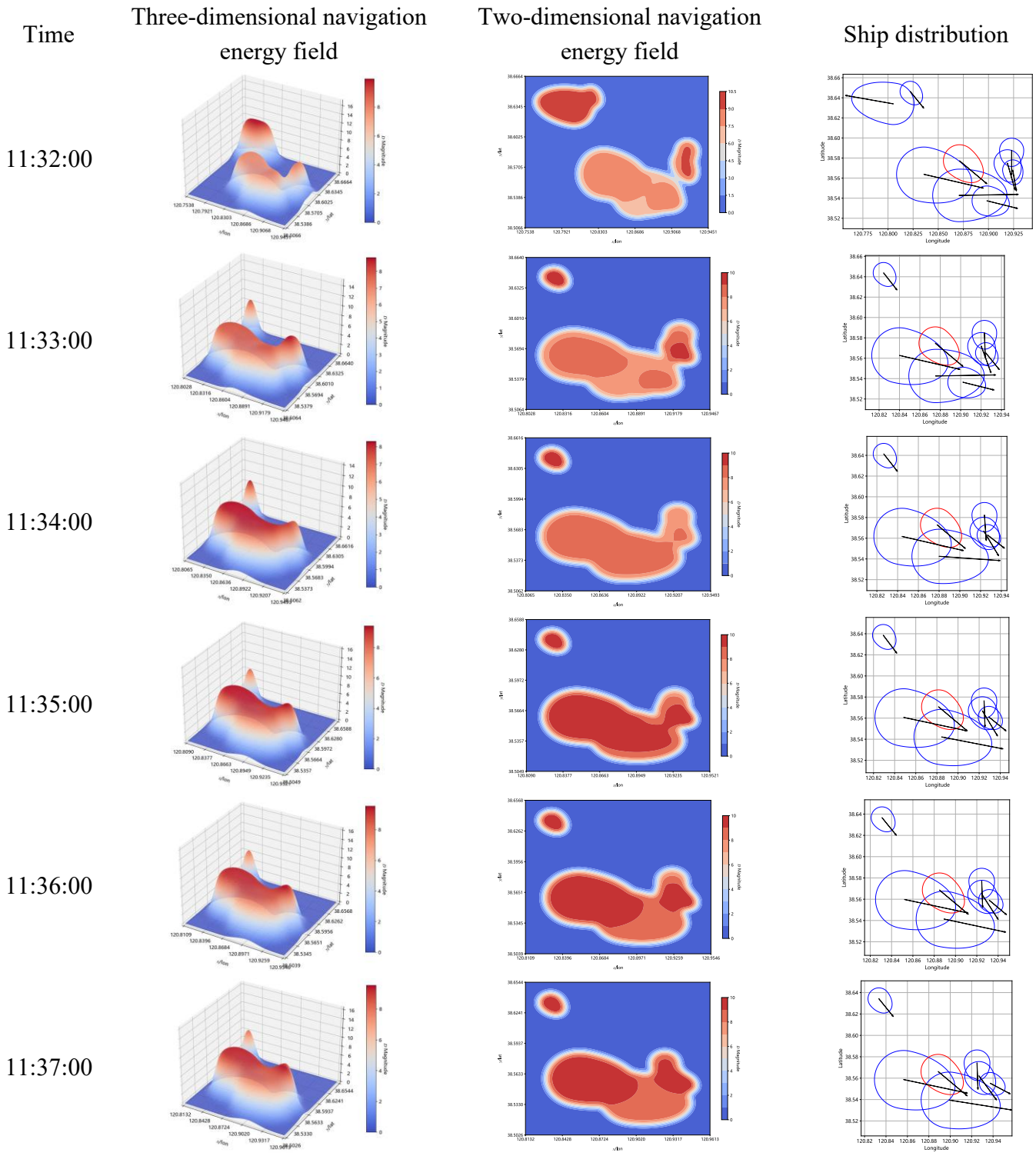

Fig. 26 Schematic diagram of the target ship B's navigation scenario during critical periods

5. Discussion

The proposed navigation energy field model, based on multi-ship interaction characteristics, demonstrated strong risk identification capabilities during case validation. Taking the maritime traffic situation depicted in Figure 26 as an example, the model accurately identified the progressive intrusion of the target ship B into the SD of other vessels and dynamically reflected the evolving trend of potential collision risk.

According to the definition of the MoO concept established by the IMO at the 107th session of the MSC, MASS must dynamically assess the need to switch MoO in response to changes in the external environment to ensure navigational safety. Addressing this requirement, the navigation energy field model constructed in this study integrates maritime traffic complexity quantification results, dynamically computing local energy distributions by coupling multi-ship interaction relationships. This allows real-time identification of risk levels in high-density traffic environments. The model not only reflects variations in local traffic risk levels but also provides decision support for adaptive MoO switching. When the risk level of a MASS continues to rise or when abnormal navigation energy field agglomeration is detected, the system can recommend triggering a downgrade from the AM to RM, OCM, or EM, thereby enhancing system robustness and navigational safety under complex conditions.

It should be pointed out that although the navigation energy field risk modelling framework proposed in this paper shows good adaptability and recognition effects in multi-ship interaction scenarios, its calculation process relies on data from conventional ship-borne perception sources such as AIS and radar, has low calculation complexity, and has certain real-time assessment potential. Therefore, it can be used as a supplement to the risk assistance judgement module in the Electronic Chart Display and Information System (ECDIS), displaying the navigation energy field distribution results through layer superposition to enhance the driver's intuitive perception of complex situations. Follow-up research can further explore the integration of this model in actual ship systems and optimize its computational performance to achieve more efficient online risk assessment capabilities.

This study has several limitations that warrant further exploration and refinement in subsequent research. The current model assumes that ship movement information is complete and accurate and does not consider the potential impact of incomplete information, such as positioning errors, on the risk calculation results. At the same time, the modelling process simplifies external environmental disturbance factors, which may significantly affect ship navigation behavior and interaction patterns in complex sea conditions. The current model assumes that ships are ideal standard ships and does not fully reflect the differences in avoidance intentions and risk sensitivity among different types of ships. The modelling process does not systematically consider the constraints of collision avoidance rules on the navigation energy field. Based on the above issues, future research can be carried out in the following areas: Introduce multi-source sensor information fusion and data repair mechanisms to improve robustness and stability in scenarios with incomplete or delayed data. Combine environmental perception models with marine meteorological disturbance modelling to achieve more realistic navigation environment simulation; establish behavioral difference models for multiple types of ships and introduce data-driven parameter adaptation mechanisms to improve versatility; consider the collaborative modelling of avoidance rules and energy propagation mechanisms to construct a ‘rule-guided risk assessment model’, which could integrates COLREGs rule-based reasoning with an energy field model, achieved through adaptive risk coefficients based on encounter types and vessel responsibilities, rule-driven threshold adjustment mechanisms, and coordination between risk perception and collision avoidance maneuver planning. In addition, follow-up research can combine actual ship trials to verify and calibrate the model to further enhance its practicality and engineering promotion value.

6. Conclusion

This study focuses on the multi-ship interaction characteristics within complex maritime traffic environments and proposes a dynamic quantitative model based on the navigation energy field theory. The core contribution is the direct integration of maritime traffic complexity into the potential function, establishing a coupled risk model that reflects both geometric proximity and interaction dynamics within a unified mathematical framework. Case validation using real AIS data was conducted to assess the model’s effectiveness. The results demonstrate that the constructed navigation energy field model effectively captures the dynamic behaviors between vessels and accurately identifies potential collision risks, exhibiting high sensitivity to risk perception and strong adaptability to diverse traffic scenarios. In particular, under high-density traffic conditions, the model dynamically analyzes the risk evolution process by real-time computation of multi-ship encounter characteristics, thereby laying the foundation for adaptive MoO switching.

Specifically, the proposed navigation energy field model not only quantifies the risk distribution characteristics within the local navigation environment but also provides technical support for the adaptive MoO switching mechanism of MASS. When the local risk level exceeds the system-defined threshold, the real-time analysis results derived from the navigation energy field can serve as a trigger condition for MoO switching, by employing specific switching logistics, guiding MASS to smoothly transition from AM to RM, OCM, or EM, thereby enhancing navigational safety in complex traffic situations.

In summary, this study develops a comprehensive framework for navigation risk assessment and MoO switching, encompassing theoretical modeling, algorithm design, and case validation, all centered on the construction and application of the navigation energy field model. The research outcomes not only offer a solid theoretical basis for adaptive MoO switching but also lay an important foundation for achieving safe and efficient navigation of MASS in real-world maritime environments.

FUNDING

This work was supported by the National Natural Science Foundation of China (Grant No. 52231014) and the Team Project of Dalian Maritime University (Grant No. 3132023511).

APPENDIX

List of symbols

$a_{ij}(t)$	the contribution of ship j to the complexity by ship i at time t	n	the number of ships
A	the traffic complexity measurement matrix	$pv_{ij}(t)$	the complexity caused by the traffic situation at time t, also named as proximity factor
$cv_{ij}(t)$	the spatial convergence factor at time t	r	the earth radius
C_{omplex}	the ship traffic complexity of ship i	R	the current sliding window interval
CI	the confidence interval of the sliding window	R_{ij}	a value contingent upon the type of ships and the navigational area
d	the distance from the ship center	s	the sample standard deviation
$den_{ij}(t)$	the complexity caused by the ship density at time t, also named as ship density	$tv_{ij}(t)$	the temporal convergence factor at time t
$d_{safedis}$	the safe distance between two ships	$v_{ij}(t)$	the relative velocity between ship i and j at time t
D_{φ}	the whole boundary of the ship domain	$w_{ij}(t)$	the weight of ship j to the complexity by ship i at time t
$D_{\varphi af}$	the after boundary of the ship domain	$z_{\alpha/2}$	the confidence coefficient
$D_{\varphi fr}$	the forward boundary of the ship domain	φ_p	the angle between point P and the bow direction of the ship
D_t	the calculated risk value of the navigation energy field at time t	λ	the lateral influence parameters of the ship domain
$ev_{ij}(t)$	the complexity caused by the difficulty of traffic mitigation at time t, also named as mitigation index	$\theta(t)$	the courses of ship at time t
g_{amma}	a tuning parameter that determines the risk value of the navigation energy field	τ	a tuning factor that emphasizes the degree of influence exerted by distance

k	a tuning parameter that determines the curvature of the function	α	a correction parameter dependent on the navigational environment of the ships
lon	the longitude of ship	$\overrightarrow{d_{ij}(t)}$	the relative distance vector between ship i and j at time t
lat	the latitude of ship	$\bar{R}$	the average risk value within the sliding window
L_i	the length of the ship	δ	the longitudinal influence parameters of the ship domain
m	the number of risk value samples in the sliding window		

REFERENCES

[1] Zhang, W., Zhang, Y., Zhang, C., 2024. Research on risk assessment of maritime autonomous surface ships based on catastrophe theory. *Reliability Engineering & System Safety*, 244, 109946. https://doi.org/10.1016/j.ress.2024.109946

[2] International Maritime Organization, 2025. Maritime Safety Committee (MSC), 99th session 16-25 May 2018. https://www.imo.org/en/mediacentre/meetingsummaries/pages/msc-99th-session.aspx (accessed 19st October 2025)

[3] International Maritime Organization, 2025. Maritime Safety Committee (MSC 107), 31 May-9 June 2023. https://www.imo.org/en/mediacentre/meetingsummaries/pages/msc-107th-session.aspx (accessed 19st October 2025)

[4] Xu, L., Huang, L., Zhao, X., Liu, J., Chen, J., Zhang, K., He, Y., 2025. Navigational decision-making method for wide inland waterways with traffic separation scheme navigation system. *Brodogradnja*, 76(2), 76201. https://doi.org/10.21278/brod76201

[5] Zhang, H., Zhang, Y., Lu, H., Niu, Y., 2024. Research on the Decision-Making and Control System Architecture for Autonomous Berthing of MASS. *Journal of Marine Science and Engineering*, 12(12), 2293. https://doi.org/10.3390/jmse12122293

[6] Wang, S., Zhang, Y., Zhang, X., Gao, Z., 2023. A novel maritime autonomous navigation decision-making system: Modeling, integration, and real ship trial. *Expert Systems with Applications*, 222, 119825. https://doi.org/10.1016/j.eswa.2023.119825

[7] Wang, S., Zhang, Y., Zheng, Y., 2021. Multi-ship encounter situation adaptive understanding by individual navigation intention inference. *Ocean Engineering*, 237, 109612. https://doi.org/10.1016/j.oceaneng.2021.109612

[8] Sezer, S. I., Ahn, S. I., Akyuz, E., Kurt, R. E., Gardoni, P., 2024. A hybrid human reliability analysis approach for a remotely-controlled maritime autonomous surface ship (MASS- degree 3) operation. *Applied Ocean Research*, 147, 103966. https://doi.org/10.1016/j.apor.2024.103966

[9] Bakdi, A., Vanem, E., 2022. Fullest COLREGs Evaluation Using Fuzzy Logic for Collaborative Decision-Making Analysis of Autonomous Ships in Complex Situations. *IEEE Transactions on Intelligent Transportation Systems*, 23(10), 18433-18445. https://doi.org/10.1109/TITS.2022.3151826

[10] Namgung, H., Kim, J. S., 2021. Collision Risk Inference System for Maritime Autonomous Surface Ships Using COLREGs Rules Compliant Collision Avoidance. *IEEE Access*, 9, 7823-7835. https://doi.org/10.1109/ACCESS.2021.3049238

[11] Qiao, Z., Zhang, Y., Wang, S., 2021. A Collision Risk Identification Method for Autonomous Ships Based on Field Theory. *IEEE Access*, 9, 30539-30550. https://doi.org/10.1109/ACCESS.2021.3059248

[12] Shin, G. H., Yang, H., 2025. Deep reinforcement learning for integrated vessel path planning with safe anchorage allocation. *Brodogradnja,* 76(3), 76305. https://doi.org/10.21278/brod76305

[13] Im, N., Luong, T. N., 2019. Potential risk ship domain as a danger criterion for real-time ship collision risk evaluation. *Ocean Engineering*, 194, 106610. https://doi.org/10.1016/j.oceaneng.2019.106610

[14] Ji, Z., Zhang, Y., Wang, F., Yang, J., Zou, Y., 2024. Identification of multi-ship maritime traffic situation based on ship traffic complexity measurement model. *Ocean Engineering*, 301, 117442. https://doi.org/10.1016/j.oceaneng.2024.117442

[15] Hurst, J., McIntyre, J., Tamauchi, Y., Kinuhata, H., Kodama, T., 2018. A summary of the "ALARP" principle and associated thinking. *Journal of Nuclear Science and Technology*, 56(2), 241-253. https://doi.org/10.1080/00223131.2018.1551814

[16] Gao, J., Zhang, Y., 2024. Ship collision avoidance decision-making research in coastal waters considering uncertainty of target ships. *Brodogradnja*, 75(2), 75203. https://doi.org/10.21278/brod75203

[17] Rodseth, O. J., Wennersberg, L. A. L., Nordahl, H., 2022. Towards approval of autonomous ship systems by their operational envelope. *Journal of Marine Science and Technology*, 27(1), 67-76. https://doi.org/10.1007/s00773-021-00815-z

[18] Liu, J., Zhang, J., Yan, X., Soares, C. G., 2022. Multi-ship collision avoidance decision-making and coordination mechanism in Mixed Navigation Scenarios. *Ocean Engineering*, 257, 111666. https://doi.org/10.1016/j.oceaneng.2022.111666

[19] Ding, J., Tseng, W. J., Sung, Y. J., 2024. An evaluation of operational risks for general cargo ship operators. *Brodogradnja*, 75(1), 75101. https://doi.org/10.21278/brod75101

[20] Fujii, Y., Tanaka, K., 1971. Traffic Capacity. *Journal of Navigation*, 24(4), 543-552. https://doi.org/10.1017/S0373463300022384

[21] Wen, Y., Huang, Y., Zhou, C., Yang, J., Xiao, C., Wu, X., 2015. Modelling of marine traffic flow complexity. *Ocean Engineering*, 104, 500-510. https://doi.org/10.1016/j.oceaneng.2015.04.051

[22] Sui, Z., Wen, Y., Huang, Y., Zhou, C., Xiao, C., Chen, H., 2020. Empirical analysis of complex network for marine traffic situation. *Ocean Engineering*, 214, 107848. https://doi.org/10.1016/j.oceaneng.2020.107848

[23] Liu, Z., Wu, Z., Zheng, Z., Wang, X., Soares, C. G., 2021. Modelling dynamic maritime traffic complexity with radial distribution functions. *Ocean Engineering*, 241, 109990. https://doi.org/10.1016/j.oceaneng.2021.109990

[24] Sui, Z., Wen, Y., Zhou, C., Huang, X., Zhang, Q., Liu, Z., Piera, M. A., 2022. An improved approach for assessing marine traffic complexity based on Voronoi diagram and complex network. *Ocean Engineering*, 266, 112884. https://doi.org/10.1016/j.oceaneng.2022.112884

[25] Zhang, F., Liu, Y., Du, L., Goerlandt, F., Sui, Z., Wen, Y., 2023. A rule-based maritime traffic situation complex network approach for enhancing situation awareness of vessel traffic service operators. *Ocean Engineering*, 284, 115203. https://doi.org/10.1016/j.oceaneng.2023.115203

[26] Tong, Y., Zhen, R., Dong, H., Liu, J., 2023. Identifying influential ships in multi-ship encounter situation complex network based on improved WVoteRank approach. *Ocean Engineering*, 284, 115192. https://doi.org/10.1016/j.oceaneng.2023.115192

[27] Qiao, Z., 2022. Collision Risk Identification for Autonomous Ships in Complex Scenes Based on Field Theory. *Master Thesis*, Dalian Maritime University, Dalian, Liaoning, China.

[28] Cai, C., 2015. Study on Ship Collision Risk based on Field Theory. *Master Thesis*, Dalian Maritime University, Dalian, Liaoning, China.

[29] Ma, X., 2024. Research on Decision-making and Model of Intelligent Ship Following in Inland Waterway Based on Safety Potential Field. *Master Thesis*, Shandong Jiaotong University, Jinan, Shandong, China.

[30] Lazarowska, A., 2020. A Discrete Artificial Potential Field for Ship Trajectory Planning. *Journal of Navigation*, 73(1), 233-251. https://doi.org/10.1017/S0373463319000468

[31] Lyu, H., Liu, W., Guo, S., Tan, G., Fu, C., Sun, X., Zhao, Y., Zhang, L., Yin, Y., 2024. Autonomous collision avoidance method for MASSs based on precise potential field modelling and COLREGs constraints in complex sailing environments. *Ocean Engineering*, 292, 116530. https://doi.org/10.1016/j.oceaneng.2023.116530

[32] DiArchangel, K., 2024. Comparing Potential Fields and Velocity Obstacles for Rules of the Road Compliant Ship Driving. *Master Thesis*, University of Nevada, Reno, Nevada, United States. https://doi.org/10.1145/3638530.3664089

[33] Zhang, W., Mu, C., Wang, Y., Yang, X., Zhou, X., Meng, X., Li, L., 2024. Exploring the MASS-DoA2 control-switching mechanism: Results from the autonomous ship guidelines review and expert survey. *Journal of Navigation*, 77(2), 276-305. https://doi.org/10.1017/S0373463324000237

[34] Li, W., Chen, W., Guo, Y., Hu, S., Xi, Y., Wu, J., 2024. Risk Performance Analysis on Navigation of MASS via a Hybrid Framework of STPA and HMM: Evidence from the Human–Machine Co-Driving Mode. *Journal of Marine Science and Engineering*, 12(7), 1129. https://doi.org/10.3390/jmse12071129

[35] Yuzui, T., Kaneko, F., 2025. Toward a hybrid approach for the risk analysis of maritime autonomous surface ships: a systematic review. *Journal of Marine Science and Technology*, 30(1), 153-176. https://doi.org/10.1007/s00773-024-01040-0

[36] Du, A., 2009. Study on Port Fairway Capacity Based on Standard Vessels. *Master Thesis*, Dalian University of Technology, Dalian, Liaoning, China.

[37] Zou, Y., Zhang, Y., Wang, S., Jiang, Z., Wang, X., 2024. Ship regulatory method for maritime mixed traffic scenarios based on key risk ship identification. *Ocean Engineering*, 298, 117105. https://doi.org/10.1016/j.oceaneng.2024.117105

[38] Zhang, W., Feng, X., Goerlandt, F., Liu, Q., 2020. Towards a Convolutional Neural Network model for classifying regional ship collision risk levels for waterway risk analysis. *Reliability Engineering and System Safety*, 204, 107127. https://doi.org/10.1016/j.ress.2020.107127

[39] Liu, T., Xu, X., Lei, Z., Zhang, X., Sha, M., Wang, F., 2023. A multi-task deep learning model integrating ship trajectory and collision risk prediction. *Ocean Engineering*, 287, 115870. https://doi.org/10.1016/j.oceaneng.2023.115870

[40] Eski, O., Tavacioglu, L., 2024. A combined method for the evaluation of contributing factors to maritime dangerous goods transport accidents. *Brodogradnja*, 75(4), 75408. https://doi.org/10.21278/brod75408